DC Collection and Transmission for Offshore Wind Farms

D2.2 Final Report

Prepared for:

The National Offshore Wind Research & Development Consortium

Stony Brook, NY

Mel Schultz

Project Manager

Prepared by:

GE Research

Niskayuna, NY

Rajib Datta

Principal Investigator

Notice

This report was prepared by Rajib Datta in the course of performing work contracted for and sponsored by the National Offshore Wind Research and Development Consortium, the New York State Energy Research and Development Authority, the U.S. Department of Energy and as applicable, other funding sources (hereafter the "Sponsors"). The opinions expressed in this report do not necessarily reflect those of the Sponsors, the State of New York, the federal government and reference to any specific product, service, process, or method does not constitute an implied or expressed recommendation or endorsement of it. Further, the Sponsors, the State of New York, and the contractor make no warranties or representations, expressed or implied, as to the fitness for particular purpose or merchantability of any product, apparatus, or service, or the usefulness, completeness, or accuracy of any processes, methods, or other information contained, described, disclosed, or referred to in this report. The Sponsors, the State of New York, and the contractor make no representation that the use of any product, apparatus, process, method, or other information will not infringe privately owned rights and will assume no liability for any loss, injury, or damage resulting from, or occurring in connection with, the use of information contained, described, disclosed, or referred to in this report.

The Consortium makes every effort to provide accurate information about copyright owners and related matters in the reports we publish. Contractors are responsible for determining and satisfying copyright or other use restrictions regarding the content of the reports that they write, in compliance with the Consortium's policies and federal law. If you are the copyright owner and believe a Consortium report has not properly attributed your work to you or has used it without permission, please email contracts@nationaloffshorewind.org. Information contained in this document, such as web page addresses, are current at the time of publication.

This material is based upon work supported by the U.S. Department of Energy's Office of Energy Efficiency and Renewable Energy ("EERE") under the Wind Energy Technologies Office Award Number DE-EE0008390."

Table of Contents

List of Figures

List of Tables

Acronyms and Abbreviations

AEP	Annual energy production
AC	Alternative current
CapEx	Capital cost
DC	Direct current
FERC	Federal Energy Regulatory Commission
FB	Full bridge
GIS	Gas-insulated switchgear
GSU	Generator step-up
HB	Half bridge
HVAC	High voltage AC
HVDC	High voltage DC
ISO-NE	Independent System Operator New England
LCOE	Levelized cost of energy
LCC	Line commutated converter
MMC	Modular multilevel converter
MVAC	Medium voltage AC
MVDC	Medium voltage DC
NERC	North American Electric Reliability Corporation
NOWRDC	National Offshore Wind Research and Development Consortium
NPCC	Northeast Power Coordinating Council
NYISO	New York Independent System Operator
NYSERDA	New York State Energy Research and Development Authority
OpEx	Operating cost
O&M	Operation and Maintenance
PF	Power factor
PoC	Point of connection
SC	Switched capacitor
STATCOM	Static synchronous compensator
SVC	Static VAR compensator
SM	Sub-module
VSC	Voltage source converter
WACC	Weighted average cost of capital

Executive Summary

This project explores a novel DC-based architecture for interconnecting offshore wind farms to the onshore grid. The proposed architecture comprises a medium voltage DC (MVDC) offshore collection system and high voltage DC (HVDC) transmission via subsea cable. The objective of the study is to establish its technical feasibility through preliminary system design, analysis, modeling, and simulation and compare it against established solutions, namely: (i) medium voltage AC (MVAC) collection and high voltage AC (HVAC) transmission and (ii) MVAC collection and HVDC transmission. In addition, a techno-economic trade-off study is also performed to understand the economic viability of the proposal.

In Task 1, a 1.2GW wind farm with 100, 12MW offshore turbines and 50 km (~30 miles) from the point of connection (PoC) onshore, is considered to compare the architectures. Preliminary system designs for all the three architectures are completed and the schematics are included in this report. A full-scale PSCAD model has been built for the AC system and steady-state power flow analysis has been performed to establish the system rating, particularly considering the significant amount of capacitive charging current required by the cable system. It is observed that the reactive power generated by the cables is ~1074MVAR at nominal voltage and requires three 220 kV 100 MVAR reactors installed in the onshore substation, three 220 kV 160 MVAR reactors on the offshore platform, and a 375 MVAR STATCOM installed at the onshore substation (preferably at the 500 kV bus) to maintain grid code compliance at the PoC and voltage levels within permissible limit at the collection system. Similar studies for the DC systems are completed and the study suggests that no reactive power support is required for the HVDC transmission cases.

In Task 2, converter topologies to convert MVDC to HVDC have being explored. Two converters are considered for this study: i) a modular multi-level (MMC) converter-based topology using similar submodules as conventional voltage-source HVDC converter, and ii) a switched capacitor (SC) based DC/DC converter with fixed voltage ratio. For the SC based converter, an in-depth modeling, cost analysis in terms of number of IGBT modules requirement and performance of the converters in present of different fault scenarios are also presented in this report.

A spreadsheet-based techno-economic analysis tool has been developed to compare the levelized cost of electricity (LCoE) between the three architectures. The comparison is primarily conducted between the cost of electrical system balance of plant (BoP), offshore platform, and operation and maintenance requirements, based on data collected from various published reports. A sensitivity analysis is also performed varying voltage levels, cost of converters and cables. Overall, the trade-off indicates a path towards reduced LCOE with the proposed architecture.

1 State-of-the-Art AC Architecture

Currently, the offshore wind farms under development in the USA have medium voltage AC (MVAC) collection system, typically at 33 kV or 66 kV, that is stepped up to 220 kV and transmitted via high voltage AC (HVAC) subsea cables. For such scenarios, typical wind turbines are rated at 6-8 MW with the average distance of the wind farm from the shore being 20-30 miles [1]. Each individual wind farm is connected to the shore via a radial feeder (Figure 1). With the increasing size of offshore wind farms (>1GW) using larger turbines (>12MW), and longer distances from the point of connection (PoC) on shore (>50 miles), the use of AC cables will result in high transmission losses and will require significant reactive power compensation. This will further increase the electrical BOP cost and may make such AC system unattractive, adversely impacting the growth of the US offshore wind industry.

1.1 Advantages and Limitations of AC based Architecture

The HVAC solution is a straightforward technical approach as both the power generated by the wind turbines and the onshore transmission grid are AC (at the same frequency) and the voltage level can be changed by adding transformers, onshore and offshore. HVAC transmission has the advantages of ease of interconnection, installation and maintenance, operational reliability and cost effectiveness for small to medium scale offshore wind farms. However, as the wind farm gets bigger and are installed farther from the onshore PoC, the disadvantages include: (i) large amount of reactive power produced in the AC subsea cables; (ii) inability to control cable and collector system voltages as the transmission distance increases; (iii) costly addition of reactive power compensation systems (shunt reactors, STATCOM, SVC, etc.) at the ends of the cable; and (iv) significantly higher losses for longer distances.

1.2 Example with AC based Architecture

A 1.2 GW wind farm example is developed to illustrate a typical AC based architecture. Figure 1 shows the architecture of the MVAC collection and HVAC transmission system. There are hundred 12 MW offshore wind turbines (WTs), each connected to a generator step-up (GSU) transformer stepping the voltage to 66 kV.

Figure 1. Example of HVAC collection, HVAC transmission system

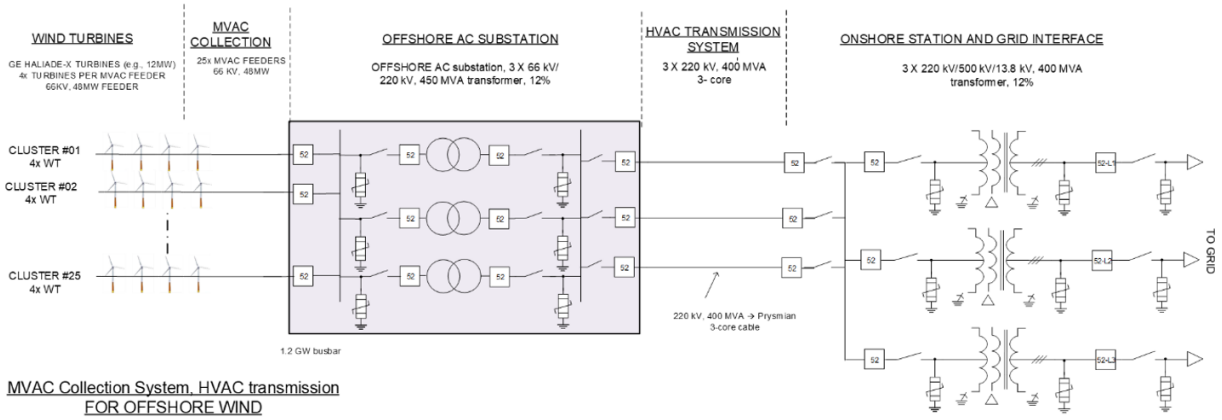

1.3 Collector System

The collector system comprises feeders of different lengths depending on the geographical layout of the wind turbines. To capture the variety in lengths of feeders, three different configurations are utilized in the proposed design shown in Figure 2. Each feeder carries four 12 MW Type-4 wind turbines. The feeders are designed such that there are a total of 25 feeders, which are aggregated as follows:

- Nine 13.5 km feeders (F1-F9) hosting 36 turbines,
- Eight 10.5 km feeders (F10-F17) hosting 32 turbines,
- Eight 7.5 km feeders (F18-F25) hosting 32 turbines.

Figure 2. Collector system one-line

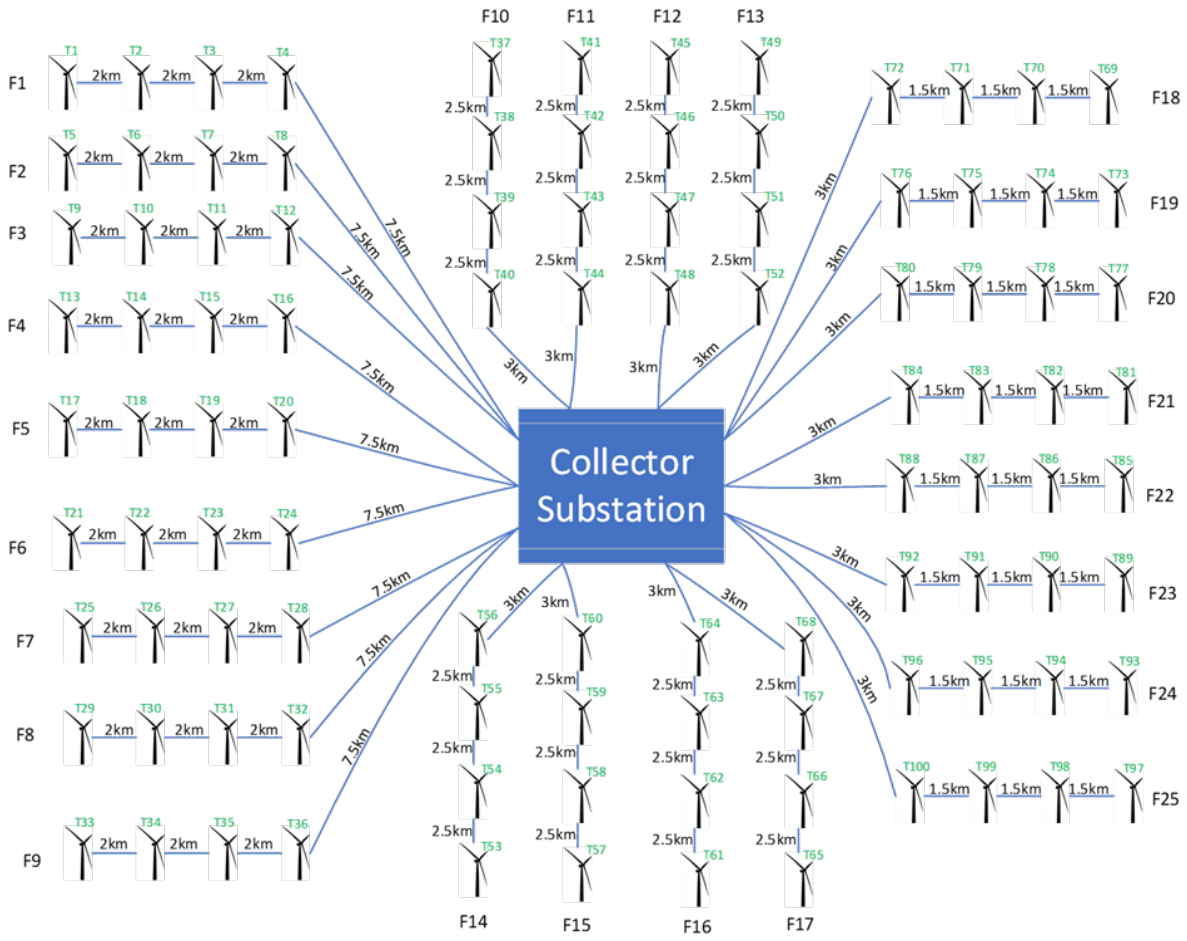

All the feeders are connected to the 1.2 GW busbar in the AC offshore platform with corresponding circuit breakers (CBs) and disconnects. Gas-insulated switchgear (GIS) is used on the offshore platform. Three transformers, each rated at 450 MVA, steps up the voltage from 66 kV to 220 kV for HVAC transmission. The transformers are designed such that they can be overloaded to 1.6 times their base ratings to deliver full output of the wind farm in case one of the three offshore transformers fails. The nameplate data for the offshore power transformers is given in Table 1.

Table 1. Offshore Transformer Nameplate Data

Number of Offshore Transformers	3
Nameplate rating (MVA)	450
Voltage ratio (kV)	220/66
Winding configuration (high/low)	Wye/Delta
Impedance (on MVA rating)	12%
X/R	60

1.4 HVAC Cable Design

From the offshore collector substation/platform, three subsea transmission cables, each rated to carry up to 450 MVA, connect the wind farm to the onshore substation. Based on the data obtained from a recent offshore wind project in Massachusetts (MA) [2] and [3], a three-core 220 kV design is chosen. In this reference wind farm (838 MW capacity) in MA, two 220 kV three-core cables are used. In comparison, the capacity of the example wind farm studied in this report is 1,200 MW; therefore, one more transmission cable is needed to increase the total cable ampacity.

The distribution cable is selected to have 50 MVA capacity so that each feeder can host four 12 MW turbines. With the voltage, design and ampacity of the cables determined, the rest of the electrical parameters are found in references [4] and [5], and listed in Table 2.

Table 2. AC Cable Parameters

Cable Type	Cross-section of conductor	Diameter of conductor	Insulation thickness	Diameter over insulation	Lead sheath thickness	Outer diameter of cable	Cable weight	Capacitance	Charging current per phase at 50 Hz	Inductance
	mm^2	mm	mm	Mm	mm	mm	kg/m	uF/km	A/km	mH/km
220 kV Transmission Cable	1600	47.4	23.0	96.8	3.1	131.8	46.0	0.22	8.6	0.37*
66 kV Collector Cable	300	20.4	9.0	40.8	1.6	134.0	34.3	0.24	2.8	0.37

*This value is updated for the trefoil formation per PSCAD calculations, as the trefoil value was not provided in [4]. Compared with a flat formation, a trefoil formation provides a lower inductance value. This is mostly due to a reduction in the induced current flowing through the sheath and armor.

At the termination of transmission cable in the onshore substation, three 400 MVA transformers are installed stepping the voltage up to EHV level. The parameters of the onshore transformers are given in Table 3.

Table 3. Onshore Transformer Data

Number of Offshore Transformers	3
Nameplate rating (MVA)	400
Voltage ratio (kV)	500/220/13.8
Winding configuration (high/low)	Wye/Wye/Delta
Impedance (on MVA rating)	12%
X/R	60

1.5 Reactive Power Compensation Methodology

The subsea cable used in the HVAC transmission system is one of the most important components of the system, as the cost of the cable represents a large fraction of the total cost of the offshore wind farm. The major problem with AC subsea cables is the large reactive power generated by the cable's high shunt capacitance, which is significantly higher than the shunt capacitance observed in overhead lines. As the cable must carry the load current and the reactive current generated by the cable capacitance, it results in reduction of the power rating of the cable.

The disadvantage escalates for longer distances and larger wind farms. This is because the cable capacitance is distributed along the length of the cable – the longer the cable, the higher the capacitance and the resulting generated reactive power. On the other hand, as the power output of the wind farm increases, the cable system voltage rating needs to be increased to minimize real power losses. This also leads to higher charging currents, worsening the situation. Another downside is, uncompensated capacitive reactive power generated by the subsea cable leads to high voltages on the remote end of the cable, which can easily exceed 110% voltage in steady-state and over 150% during switching transients. Energization of the collector system might not be possible when the remote end voltage is above the maximum allowable voltage limits.

To limit voltage rise and reduce charging current produced by a subsea cable, a common design practice is to compensate 70 to 80% of cable charging, accomplished by adding shunt reactors on both terminals of a transmission cable [6]. In offshore wind applications, there are two feasible locations where shunt reactors could be installed:

1. At the cable termination on the offshore platform, which is also the high side of the offshore power transformer.
2. At the cable termination in the onshore substation. If there is another voltage transformation (e.g., 220 to 500 kV) needed for transmission interconnection, then the cable termination is on the low side of the power transformer along with the shunt reactor.

For the example 1.2 GW wind farm, assuming each transmission cable is 80 km long and the total collector system cable length is 265.5 km per the design given in Figure 2, the line charging values are calculated using the line constants program in PSCAD and the collector system aggregation methodology developed by NREL [7]. The results are summarized in Table 4.

Table 4. Capacitive Reactive Power Generated by Cables

Feeder Aggregation	No. of Turbines	Distribution Cable		Transmission Cable		Total Reactive Power
		Length (km)	Reactive Power – Charging (MVAR)	Length (km)	Reactive Power – Charging (MVAR)	MVAR at Nominal Voltage
Aggregate #1	36	121.5	48	80.0	323	371
Aggregate #2	32	84.0	33	80.0	323	356
Aggregate #3	32	60.0	24	80.0	323	347
Total	**100**	**265.5**	**105**	**240.0**	**969**	**1074**

As shown in Table 4, the total reactive power generated by all the cables at the rated voltage is 1074 MVAR. Per the earlier discussion in this section, shunt reactors need to be installed to a) compensate 70-80% of the total reactive power generated, b) to keep the open-end voltage below a certain threshold (1.05 pu is picked here, which is further explained in the simulation section below). In addition, dynamic reactive power compensation devices (STATCOM or SVC) are required when the wind turbine capability by itself is not sufficient to deliver the required reactive power at the PoC, dictated by the grid code of the host utility or system operator. The details of shunt reactor and STATCOM sizing are covered in the simulation sections below.

1.6 PSCAD Model of AC based Architecture

To perform engineering and tradeoff analyses, a power system model of the example 1.2 GW wind farm is built. The results of simulations from the AC based architecture will be compared with the results obtained for other architectures tested in subsequent sections. Using PSCAD, an electromagnetic transient (EMT) model of the wind farm is developed as shown in Figure 3.

Figure 3. PSCAD model of the wind farm for the HVAC architecture

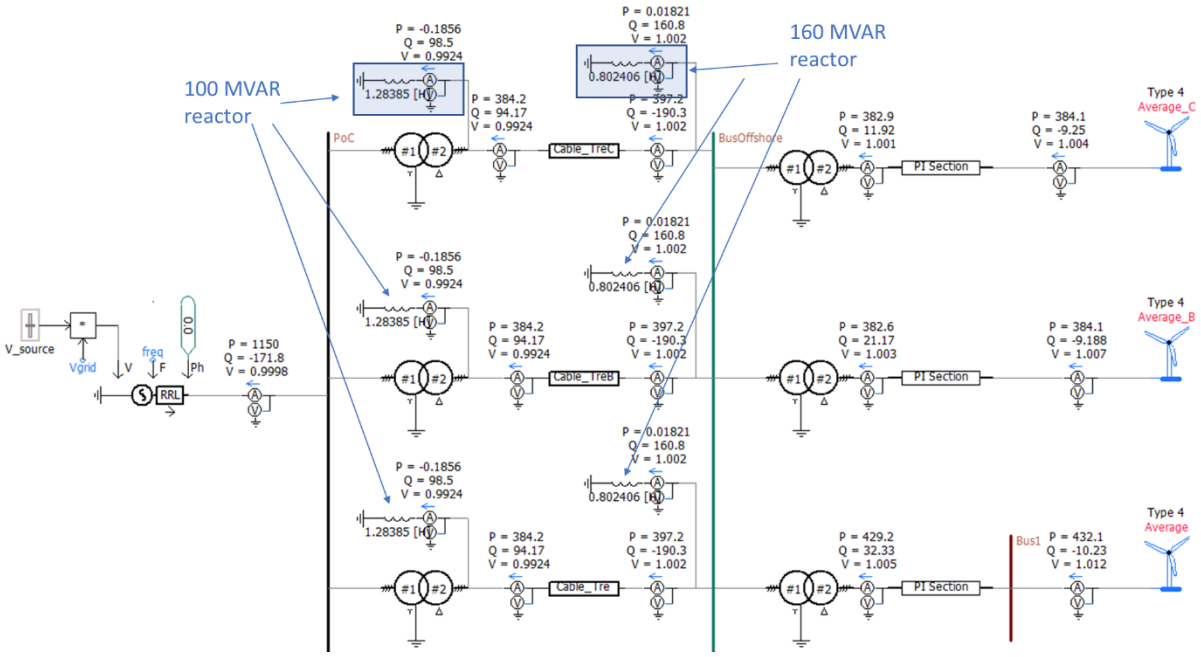

Starting from the right in Figure 3, the turbines are grouped into three aggregates. The first aggregate in the bottom represents 36 turbines while the aggregates B and C represent 32 turbines each. Aggregation is necessary since it will be computationally challenging to model all hundred turbines individually. PSCAD's native scaling component, which multiplies the output of a single turbine to a given number of turbines, is used to create the turbine aggregates. Going from right to left, the next set of components corresponds to the PI sections for the collector cables of each aggregate. In PSCAD, the most accurate way to model cables is to use the frequency-dependent component, especially for longer cables (e.g., greater than 20-30 miles). However, since each of the 25 feeders is relatively short (13.5 km or less), a PI model provides a good approximation of the collector cables, which is created using the NREL methodology [7]. The PI sections are connected to the three 450 MVA offshore transformers modeled according to the parameters given in Table 1. The only other offshore components in the model are the three 160 MVAR shunt reactors (the sizing of offshore reactors is covered in the next section) installed to compensate for cable charging.

Three 80 km subsea transmission cables connect the offshore platform to the onshore substation. The parameters in Table 2 are entered into the frequency-dependent cable model in PSCAD to represent the transmission cables. There are also three 100 MVAR shunt reactors in onshore substation compensating for cable charging. Lastly, three 400 MVA transformers step the voltage from 220 kV to 500 kV for

utility interconnection. The point of connection busbar is labeled as “PoC”. Although not shown in Figure 3, this wind farm needs three STATCOMs at the PoC to meet the grid code requirements. The simulations in the next section describe both the shunt reactor and STATCOM sizing methodology.

1.7 Simulation Results – AC Based Architecture

The analysis of the example wind farm using the AC based architecture is grouped into two sets of simulations. The first set focuses on the intra-wind farm performance to ensure that no equipment limits (thermal, voltage, safety) are exceeded. The second set focuses on the wind farm’s ability to meet the requirements of a typical grid code in North America.

1.7.1 Intra-Wind Farm Performance

During normal operation of the wind farm, it is important to ensure that no equipment limits are exceeded. Since the cables and transformers are sized to meet the full capacity of the wind farm, no thermal limitations are expected during normal operation. During equipment outages (i.e., outage of one of the offshore power transformers), some thermal ratings could be exceeded or relaxed for short duration after proper evaluation. Several scenarios are considered in this evaluation:

1. Energization of the wind farm without shunt reactors,
2. Energization of the wind farm with shunt reactors,
3. Operation of the wind farm at full output with turbines set at unity power factor.

As discussed in Section 1.5, the voltages in the collector system need to be below the high voltage limits. In addition, the cable charging needs to be compensated (usually 70-80%). As shown in Figure 4, when one of the aggregated feeders is energized without any reactors, while the wind turbines are offline, voltages above 1.19 pu are observed in the collector system. Typically, the medium voltage equipment is rated up to 1.1 pu in steady state. Therefore, this scenario shows a violation of voltage limits. In addition, there is about 408.6 MVAR reactive power (generated by the cables) being exported to the grid, which could lead to high voltages in the utility system.

Figure 4. Energization of the wind farm without shunt reactors

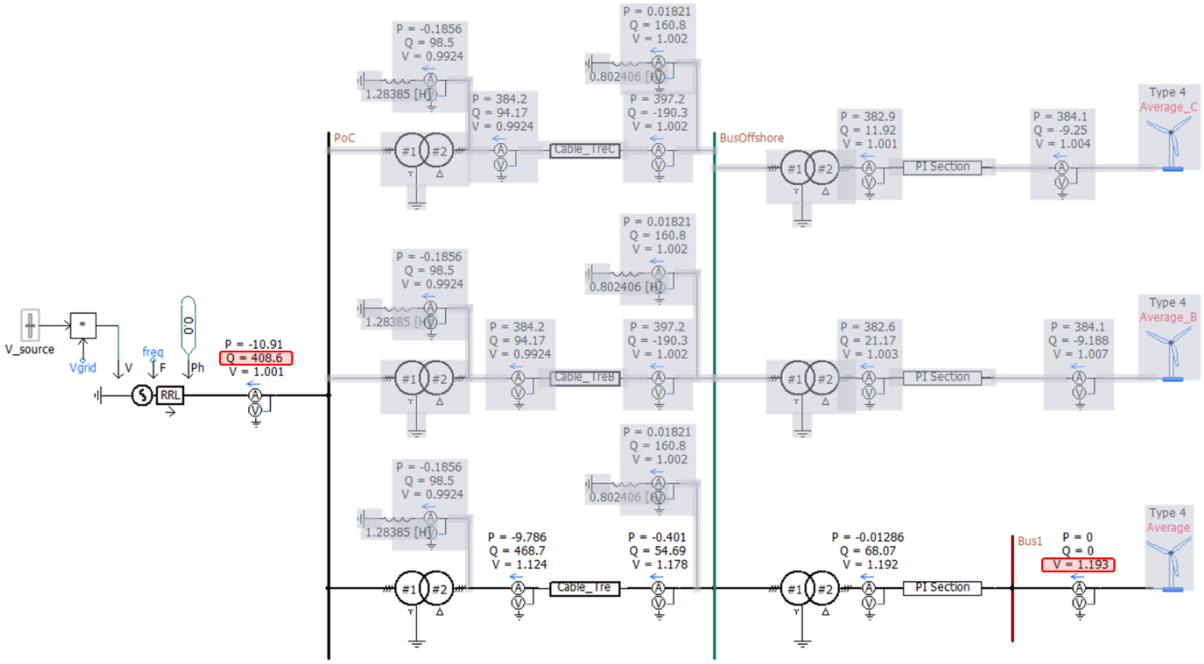

In Table 4, it is shown that the total reactive power generated by the transmission cable at nominal voltage is 371 MVAR for the first aggregated feeder. Using the design principle of 70-80% shunt compensation, a total of 260 MVAR (~70% of 371) reactors are added, 100 MVAR in the onshore substation and 160 MVAR on the offshore platform as shown in Figure 5.

Figure 5. Energization of the wind farm with shunt reactors

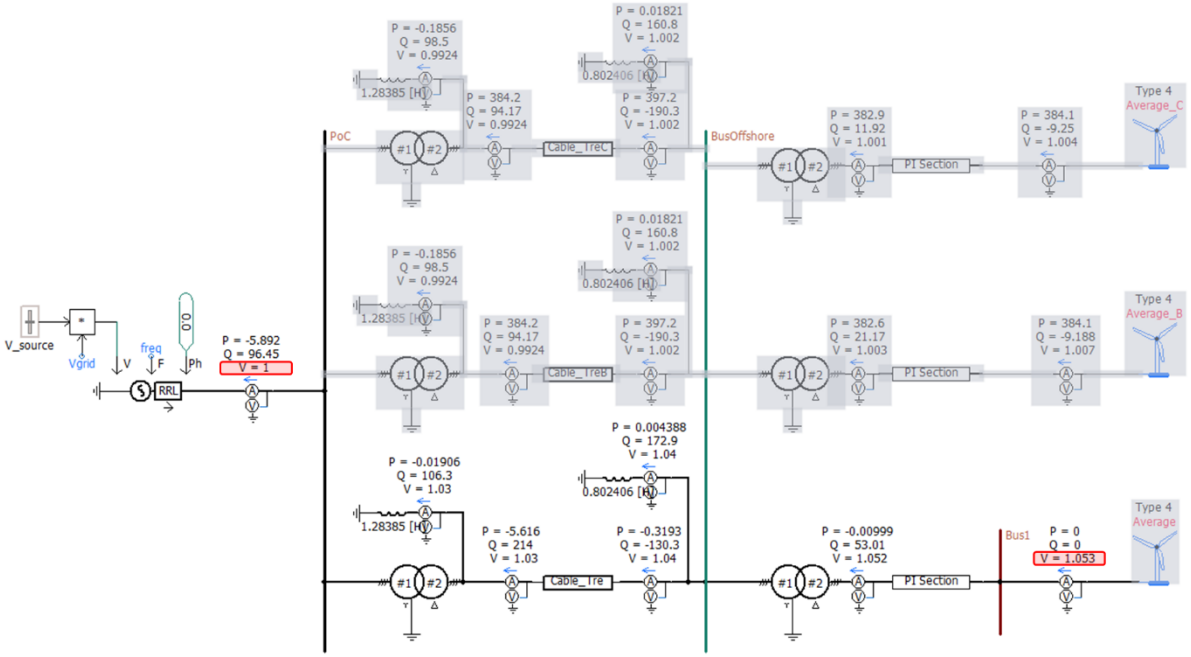

The reactor on the offshore platform (160 MVAR) is chosen to be larger than the one in the onshore substation (100 MVAR) since the offshore reactor needs to compensate both for the collector cables and the transmission cable. With about 70% compensation, the collector system voltages are reduced to about 1.05 pu. Although the typical limit for the medium voltage equipment is 1.10 pu, it is beneficial to be some margin away from this limit since the utility can operate their transmission system anywhere from 0.95 pu to 1.05 pu. With a total of 260 MVAR reactors, in addition to reducing the wind farm voltages to acceptable ranges, the reactive power exported to the system is reduced from 408 MVAR to 96 MVAR. The MVAR export can be further controlled after the installation of a STATCOM at the PoC.

Figure 6. Operation of the wind farm at full output with turbines set at unity power factor

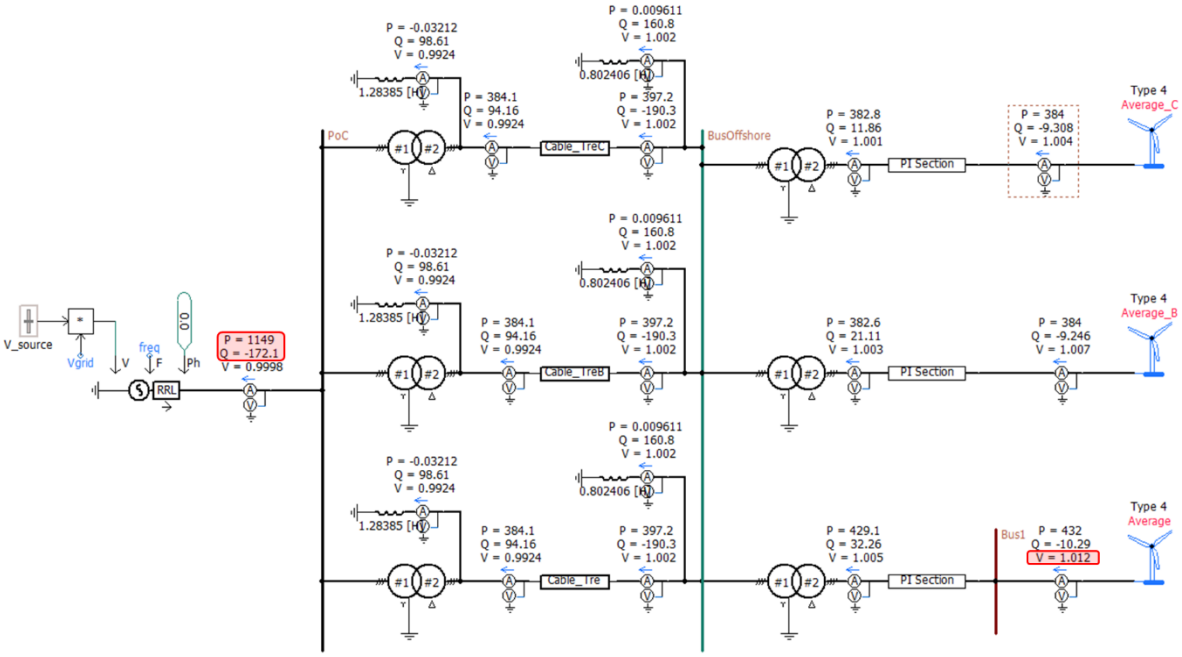

Lastly, the full output operation of the wind farm with turbines operating at unity power factor is shown in Figure 6. A couple of observations from this simulation are:

a) Although the generators are at full output (1,200 MW), the net real power injection at the PoC is about 1,150 MW due to system losses.
b) Utilities enforce wind farm reactive power requirements at the point of connection; therefore, the requirements will be based on 1,150 MW net injection.
c) At unity power factor, voltages across the wind farm are well maintained around 1.0 pu.
d) The wind farm goes from exporting reactive power to absorbing 172 MVAR reactive power while the turbines are at unity power factor.

1.7.2 Impact of AC Cable Length on Reactive Power Compensation

As described in Section 1.5, charging current of subsea cables increase as they get longer. There are three limiting factors for AC power transmission that need to be evaluated as a function of cable length:

1. thermal limitation: maximum amperage a cable can carry,
2. voltage limitation: not to exceed operating voltage limits (typically 1.05pu) at cable terminals and cable voltage hardware limit (typically 1.1 pu) at any point along the cable (e.g., midpoint),
3. stability limitation: real power transfer not to exceed the stability threshold (typically, 70% of maximum transfer limit).

Compared with transmission lines, transmission cables have high surge impedance loading (SIL), usually much higher than their thermal ratings. The surge impedance Z_C and SIL are given by the following equations:

$$Z_C = \sqrt{\frac{L}{C}}$$

$$SIL = \frac{V_0^2}{Z_C}$$

where L and C are per phase line inductance and capacitance, respectively; and V_0 is line to line voltage. The transmission cable parameters are calculated using the parameters from Table 2 according to formulas above, which result in Z_C = 41 ohms and SIL = 1176 MVA. Since there are three 220 kV cables in parallel total SIL comes out to 1176 x 3 = 3528 MVA. When transmission lines/cables are operated below their SIL, they export reactive power to the grid. With the 1200 MW rating of the wind farm being much smaller than SIL of ~3500 MVA, the three cables will be exporting large amount of reactive power at any output level from 0 MW to 1200 MW. In addition, as cable length increases, the charging current can lead to both high voltage violations (usually at midpoint if both terminals are compensated with shunt reactors) and thermal limit violations. Therefore, the relationship of cable length with cable charging current needs to be evaluated to figure out the maximum cable length. Powerflow equations are used for this analysis. The real power (P_R) and reactive power (Q_R) equations for receiving end is given by the following equations [6]:

$$P_R = \frac{E_S E_R}{Z_C \sin\theta} \sin\delta$$

$$Q_R = \frac{E_R(E_S \cos\delta - E_R \cos\theta)}{Z_C \sin\theta}$$

where E_S, E_R represent sending and receiving end voltages, respectively; δ is the angle difference between sending end and receiving end; θ is line angle, which is equal to phase constant (β) multiplied by line length (l); and Z_C is the surge impedance. Swapping E_R and E_S, the same equations can be written for the receiving end.

Forcing $E_S = E_R = 1.0$ pu, by placing shunt reactors of appropriate amount on both onshore and offshore terminals, would give a decent approximation of how HVAC subsea cables operate in offshore wind farm applications since operators are responsible to keep transmission voltages in a tight band (e.g., 1.0 pu – 1.05 pu). In addition, the relationship of cable length with voltage along the cable (from sending end to receiving end) needs to be studied for line energization (zero power transfer) scenario, which constitutes the worst-case condition for voltage violations due to high charging current. Using the powerflow equations above, this relationship is plotted for three cable lengths (80, 160 and 250 km) in Figure 7.

Figure 7. Voltage along the cable as a function of cable length with $E_S = E_R = 1.0$ pu

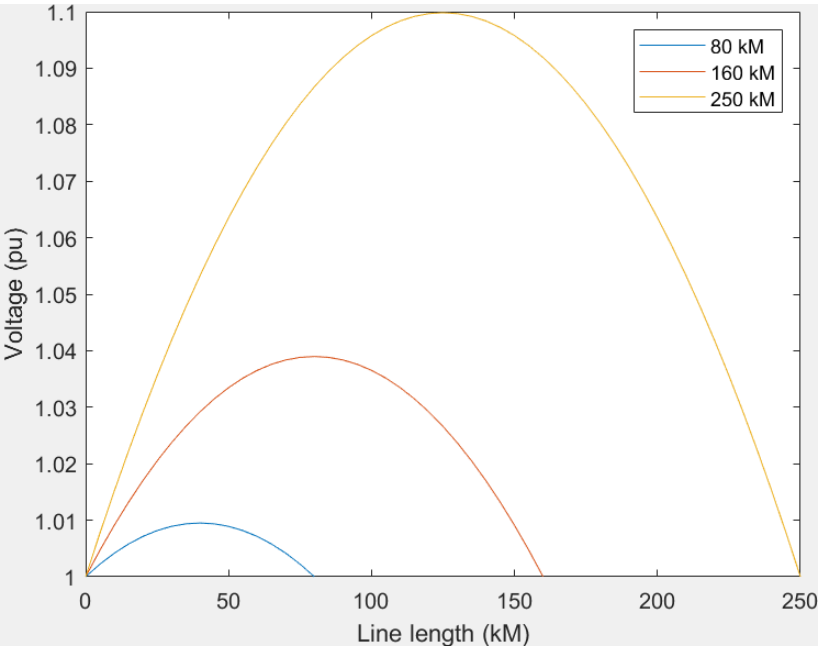

As the curve for 250 km cable shows, the midpoint voltage reaches the cable high voltage rating of ~1.1 pu. To evaluate the impact of reactive compensation in the middle of the line, the shunt reactor on the offshore terminal can be replaced by a reactor in the middle of the line. Using the powerflow equations above, a similar curve for an 80 km cable (with a reactor placed in the middle at 40 km) is shown in Figure 8.

Figure 8. Voltage along the cable as a function of cable length ($E_S = E_{mid} = 1.0$ pu)

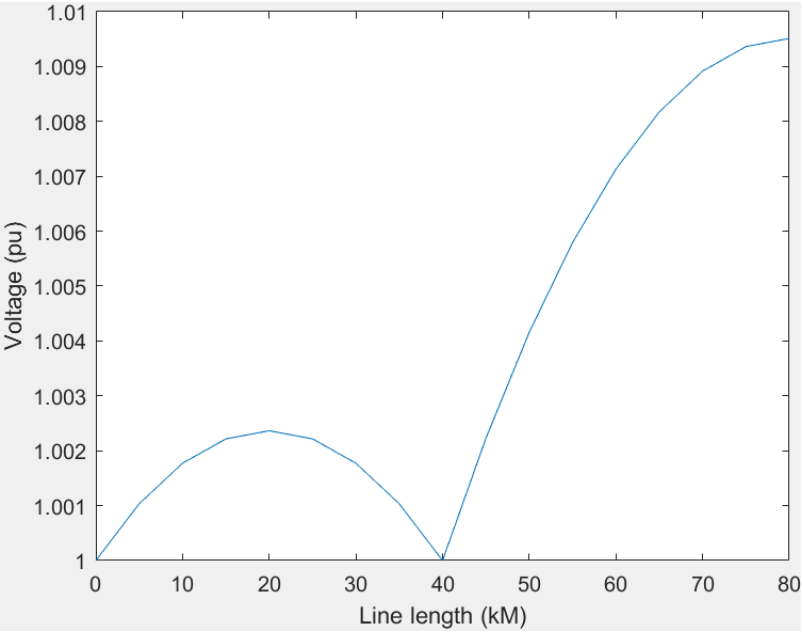

Comparing Figure 7 and Figure 8 for the 80 km cable, the highest voltage observed is the same both for remote end and midpoint reactive compensation. The only difference is that the highest voltage is at the midpoint of the line in Figure 7, whereas the highest voltage is at the remote end in Figure 8. Although not shown in Figure 8 (for simplicity), the value of highest voltage, 1.04 pu and 1.1 pu, is the same both for 160 and 250 km cables, respectively. Reactive compensation in the middle of the line is usually cost prohibitive since it requires another offshore platform. Although not studied in this section due to prohibitive cost, longer HVAC cables would be possible if reactive compensation is further increased from only two points of compensation to three: sending end, receiving end and midpoint.

Per the cable voltage limit criterion analyzed using powerflow equations above, if cables are properly compensated with shunt reactors, it is shown to be possible to go up to 250 km before a high voltage violation (i.e., 1.1 pu) is reached anywhere along the cable. Next, the thermal rating of the cable needs to be evaluated to see if it undercuts the voltage driven limit. For a more systematic and accurate analysis that includes resistive losses, a simplified two-bus model is built in powerflow software (PSAT) as shown in Figure 9.

Figure 9. Simplified 2-bus model for subsea cable length analysis

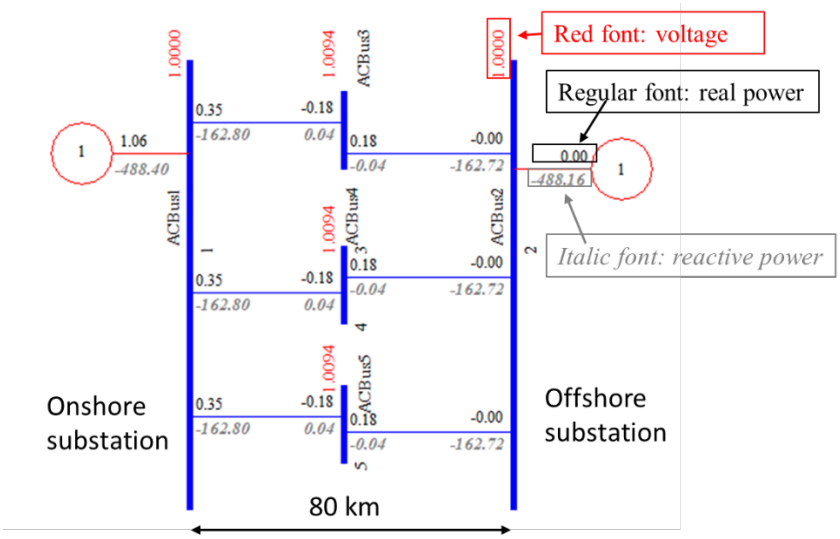

The voltage sources on the left and right in Figure 9 represent the grid connection point and the offshore substation, respectively. In this analysis, the voltage sources are assumed to have enough reactive power capability to keep their terminals at 1.0 pu voltage. Although this simplifying assumption is not realistic as the terminal voltages could vary (+/- 5%) due to system conditions, it is still useful to get a general assessment of reactive power characteristics of a transmission cable [6]. The three HVAC cables (each rated 450 MVA, 1200 A per Section 1.4) are explicitly modeled with each cable split in the middle to expose the midpoint voltage. The cable parameters (R, X, B) are calculated using PSCAD's line constants program for three cable lengths: 80, 160 and 250 km. A two-stage approach is taken to assess cable performance and reactive power compensation:

1. The real power transfer is set to 0 MW to figure out how much reactive compensation is needed to keep cable terminals at 1.0 pu. This step also reveals how high the midpoint voltage gets during line energization.
2. With the reactive shunt compensation determined in the first stage, the offshore terminal is fixed at this value and power transferred is increased from 0 MW to 1200 MW. Note that the onshore side is still regulated to 1.0 pu to represent utility interconnection. The offshore terminal voltage will move naturally since the reactive compensation is fixed at the value from Stage 1.

The results of this two-stage analysis are given in Table 5. The midpoint voltage matches the values obtained in Figure 7 with 250 km value exceeding 1.1 pu. On the other hand, the thermal rating of 1200 A is exceeded quite sooner than 250 km. The relationship of cable length with both voltage and current limits, using the data in Table 5, is plotted in Figure 10. The intersection of blue solid line with the dashed

line is around 110 km, which constitutes the thermal limit. Similarly, the intersection of the solid orange line with the dashed line is around 230 km, which constitutes the voltage limit.

Table 5. Powerflow Results for Varying Cable Length (80, 160 and 250 km)

Length (km)	Wind Output (MW)	Vgrid (pu)	Vmid (pu)	Voffshore (pu)	Offshore-Reac (MVAR)	Grid-Reac (MVAR)	Vm-Reac (MVAR)	Current (A)
80	0	1.000	1.009	1.000	488	488	0	427
80	1200	1.000	1.017	1.018	488	400	0	1113
160	0	1.000	1.038	1.000	999	1000	0	875
160	1200	1.000	1.050	1.030	999	870	0	1325
250	0	1.000	1.094	1.000	1674	1680	0	1469
250	1200	1.000	1.114	1.049	1674	1593	0	1717

Figure 10. Cable length vs voltage and thermal limits

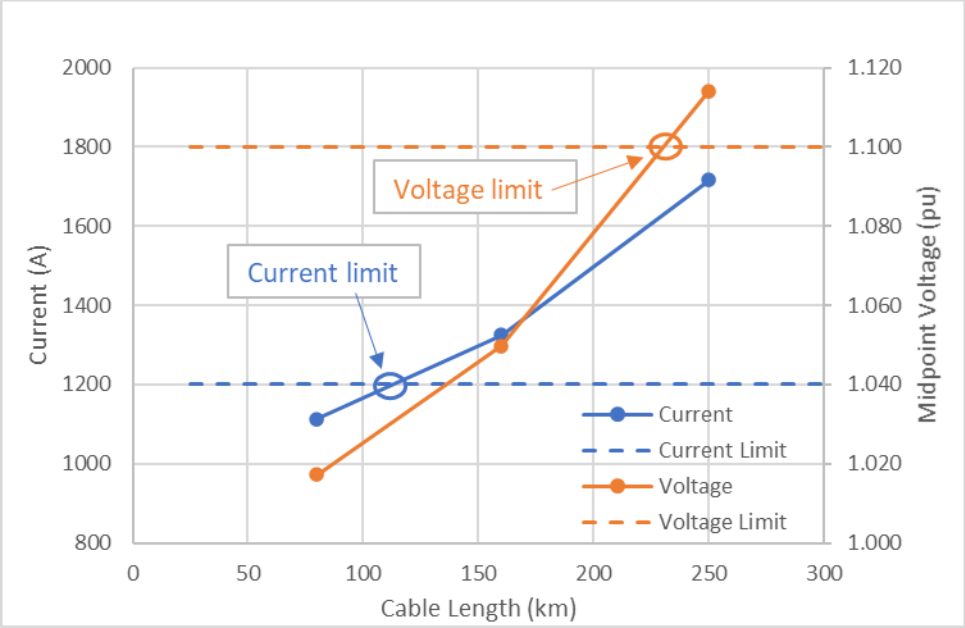

Lastly, stability criterion can be evaluated by checking the angle difference between the sending and receiving ends of the cable. Per the power transfer equation given earlier in this section, power transfer is a function of *sinδ*, which increases from 0 to 90 degrees. Although the maximum power transfer is theoretically obtained at 90 degrees, power transfer needs to be limited to 70% of the maximum value, which corresponds to δ of 44 degrees ($\sin^{-1} 0.7 = 44°$) [6]. Checking the powerflow case for the 250 km case at 1200 MW transfer, δ value is just under 13 degrees. Therefore, there are no transient stability concerns at this power level, which is typically expected when lines are loaded under their SIL.

In the next section, to ensure the wind farm meets North American grid code requirements, further simulations are presented for various operating conditions.

1.7.3 Performance of the Wind Farm at the PoC

Although the intra-wind farm equipment limits are well maintained as discussed in the previous section, it is also required to meet certain performance objectives at the PoC. There are many aspects of grid codes that vary depending on the territory and hosting utility. In North America, FERC, NERC, regional coordinating councils (i.e., NPCC in the northeast), local system operators (e.g., NYISO, ISO-NE) and utilities set the standards, criteria, and assumptions for generator interconnections. A few of the common requirements for non-synchronous generators in North America are:

1. Power factor requirement from FERC Order 827 [8]: Maintain a composite power delivery at continuous rated power output at the PoC at a power factor (PF) within the range of 0.95 leading to 0.95 lagging.
2. Dynamic reactive power requirement from FERC Order 827 [8]: Non-synchronous generators may meet the dynamic reactive power requirement by utilizing a combination of the inherent dynamic reactive power capability of the inverter, dynamic reactive power devices (e.g., Static VAR Compensators), and static reactive power devices (e.g., capacitors) to make up for losses.
3. Ability to operate within thermal and voltage limits and setpoint determined by the system operator. An example operating procedure can be found on ISO New England's website [9], which shows that the utilities in New England should be able to keep the transmission voltages within a certain range (mostly 0.95 to 1.05 pu). In addition, another operating procedure (OP12) requires generators to have certain reactive power reserves to be utilized in system operations as needed [10].

Several simulations are run to evaluate compliance against the criteria listed above. The results are given in Table 6.

Table 6. Grid Code Compliance Simulations for STATCOM Sizing

Scenarios	Total Turbine P (MW)	Total Turbine Q[1] (MVAR)	Turb Term. Volt.[2] (pu)	Power Factor at the Turb. Term.	PoC P (MW)	PoC Q (MVAR)	PoC Power Factor	PoC Volt. (pu)	Reac. Power Def.[3] (MVAR)
Full output, 0.95 lagging PF	1200	184	1.072	0.988	1151	79	0.998	1.000	**299**
Full output, 0.95 leading PF	1200	-247	0.930	-0.980	1142	**-475**	-0.924	1.000	Exceeds -378 MVAR
25% output, 0.95 lagging PF	308	103	1.074	0.949	287	326	0.962	1.000	**52**
25% output, 0.95 leading PF	308	-368	0.933	-0.642	287	-193	-0.986	1.000	**-185**

[1]Note that the turbine Q output can be limited by the terminal voltage limit before reaching 0.95 PF.
[2]The highest terminal voltage of the three aggregated turbines is reported.
[3]Reactive power requirement is calculated for 1,150 MW injection regardless of the actual real power output. The PF requirement of 0.95 corresponds to +/- 378 MVAR reactive power delivered at the PoC.

The results in Table 6 cover two real power levels: full output and 25% output. For each power level, two reactive power setpoints are tested to see if the wind farm can meet the +/- 0.95 PF requirements, which correspond to +/- 378 MVAR reactive power at the PoC. In all simulations, the PoC voltage is maintained at 1.0 pu. The turbines can typically operate from 0.9 to 1.1 pu voltage at their terminals. Although the simulations can be repeated for different PoC voltages (e.g., 0.95, 1.05 pu), some of this PoC voltage variability can be captured by limiting the turbine terminal voltages to a slightly narrower range (e.g., 0.925 to 1.075 pu) than their full voltage range.

At 1,150 MW net injection, the 0.95 leading and lagging requirement corresponds to a dynamic range of +/- 378 MVAR. Note that the dynamic reactive power requirement applies when all turbines are online even if the plant output is reduced due to low wind conditions.

A practical way to test this capability is to push the turbines to their maximum capabilities and observe if the reactive power delivered at the PoC exceed +/- 378 MVAR. As the turbines attempt to deliver their full reactive power capabilities, their terminal voltages limit first in three out of the four rows in Table 6. Only the full output, 0.95 leading PF test shows that the reactive power delivered (-474.7 MVAR) exceeds the requirements (-378 MVAR). In all other tests, the reactive power falls short of the PF requirement.

When a wind farm falls short of the dynamic PF requirements, a common solution is to install a STATCOM to make up the reactive power deficiency. The last column in Table 6 provides the amount of

reactive power needed to achieve full compliance. The largest deficiency of 299.1 MVAR is seen for the full output, 0.95 lagging PF test. Although the STATCOM size can be rounded up to 300 MVAR, it would be prudent to add some margin to cover scenarios where the STATCOM reactive power injection can result in further increase in collector system voltages (reducing turbine reactive power). With 25% margin, the STATCOM size increases to 375 MVAR. The total reactive power compensation for the AC architecture is summarized as:

1. Three 220 kV 100 MVAR reactors installed in the onshore substation,
2. Three 220 kV 160 MVAR reactors installed on the offshore platform,
3. One 375 MVAR STATCOM installed at the onshore substation (preferably at the 500 kV bus).

These additional reactive power devices increase the total cost of the AC based wind farm. The cost analysis is captured in Section 4.

1.8 Key Takeaways – AC Architecture

The HVAC architecture is the most established technical approach for wind farm interconnections. The main advantages of HVAC are a) ease of interconnection, installation and maintenance, b) operational reliability, and c) cost effectiveness for small to medium scale offshore wind farms. However, as the wind farm gets larger, the amount of reactive power compensation devices (shunt reactors, SVCs, STATCOMs) needed can become cost prohibitive. Besides cost, as the transmission cable length increases, voltage and stability limits are introduced [6]. These limits are due to either Ferranti effect or excessive line angle difference between sending and receiving ends. Therefore, unless the cables can be terminated at their surge impedance, there is a technical limit on the length of transmission cables.

2 HVDC Architecture

In a typical HVDC architecture for offshore windfarms (e.g., Dolwin3, Germany), the turbines produce power at MVAC at 50/60Hz, the voltage is then stepped up to HVAC followed by conversion to HVDC by an offshore AC-DC converter station. It is then transmitted via a HVDC subsea cable and converted back to AC by an onshore converter station. This process requires several conversion steps from the generator output to the final onshore grid connection.

2.1 Example with HVDC Architecture

Figure 11 shows a typical architecture of an MVAC collection and HVDC transmission system. The example of 1.2 GW wind farm is considered with 100, 12 MW WTs. Similar to the previous case, an example of 4 WTs connected to each feeder is considered, so the farm constitutes 25 feeders. The details of the collector system design are covered in Section 1.3. All the feeders are connected to the 1.2 GW busbar in the offshore platform with corresponding circuit breakers and disconnects. 2 transformers, each rated at 700 MVA, steps up the voltage from 66 kV to 220 kV. The transformers are rated such that in case of an outage of one, the other can be safely overloaded to carry most of the wind farm output.

Table 7. Offshore Converter Transformer Nameplate Data

Number of Offshore Transformers	2
Nameplate rating (MVA)	700
Voltage ratio (kV)	220/66
Winding configuration (high/low)	Wye/Delta
Impedance (on MVA rating)	10%
X/R	60

The two transformers connect directly to the modular multilevel converter (MMC) platform in the same offshore platform. The transformer and the MMC are integrated into the same offshore platform. The 220 kV AC input is converted to +/-320 kV HVDC and is transmitted via two 320 kV HVDC subsea cables.

In the onshore substation, the HVDC is converted back to 220 kV AC. From there, three 500 kV/ 220 kV/ 13.8 kV 400 MVA transformers, associated disconnects, CBs, and control and protection, connect the wind farm to the PoC. These onshore transformers are the same as the ones used in the HVAC solution given in Table 3.

Figure 11. Example of MVAC collection, HVDC transmission system

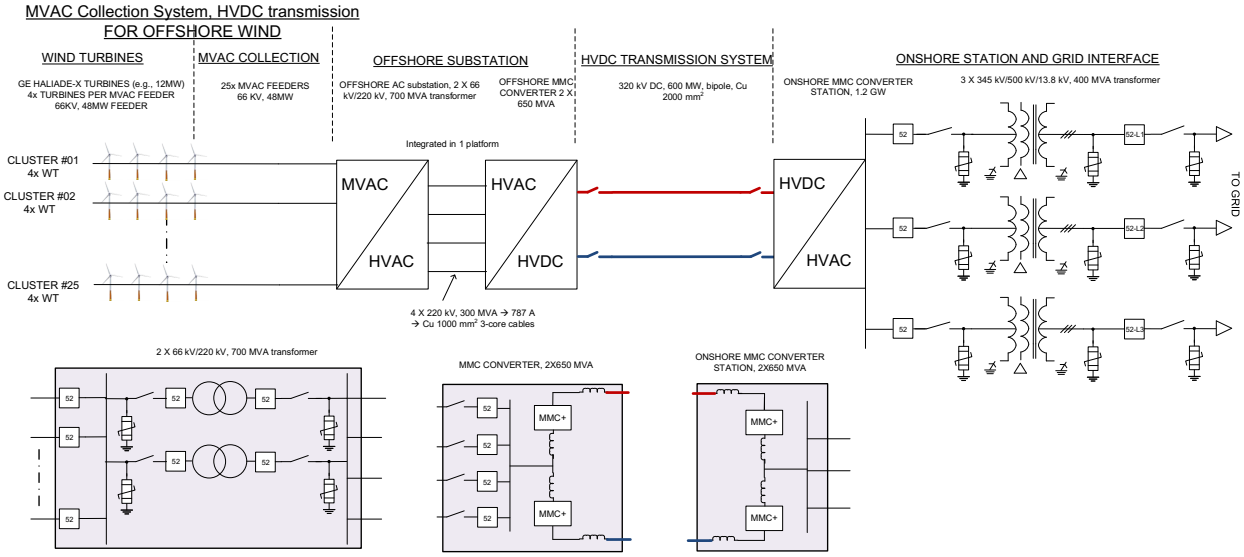

2.2 HVDC Cable Design

The outputs of the offshore MMC converters connect to the two subsea HVDC cables. In the bipolar MMC design, one pole operates at +320 kV while the other pole runs at -320 kV. Each cable is rated to carry greater than 1,875 A (600 MVA at 320 kV). With the voltage, design and ampacity of the cables determined, the rest of the electrical parameters are found in reference [11], and listed in Table 8.

Table 8. HVDC Cable Parameters

Cable Type	Cross-section of conductor	Ampacity	Diameter of conductor	Insulation thickness	Diameter over insulation	Lead sheath thickness	Outer diameter of cable	Cable weight (copper)	Capacit-ance
	mm^2	A	mm	mm	mm	mm	mm	Kg/m	uF/km
320 kV HVDC Cable	2000	1953	53.0*	25.0*	107.1*	3.1*	140.0	53.0	0.23*

*These values are estimated by comparing 2000 mm^2 cables for HVAC cables in [5] to HVDC cables in [11].

2.3 Voltage Source Converter Technology for HVDC

The voltage source converter (VSC) technology using insulated gate bipolar transistors (IGBT) has been introduced in HVDC since the 2000's. Compared to the conventional line commutated converter (LCC), VSC has the advantage of black startup capability, improved power quality, smaller footprint as well as faster and independent active and reactive power control, making it suitable for the grid integration of renewable assets.

State-of-the-art VSC-based HVDC uses series staked power conversion submodules (SM) either in full bridge (FB) or half bridge (HB) configuration as shown in Figure 12. With such modular multilevel converter (MMC) topology, quasi-sinusoidal voltage waveforms can be created, and no filter is required for connection to the grid. This is of particular importance for segments of the market where space is at a premium such as offshore platforms. Compared to the HB submodules, the FB submodules can provide fault current blocking capability with the help of additional switching devices within each SM as shown in Figure 12 (b) and (c). Each phase of a HVDC converter, consists of hundreds of SMs to reach the desired voltage level. Typically, HB submodules are more commonly used in MMC-HVDC projects; the additional switching devices of FB could result in higher cost and lower efficiency.

Figure 12. (a) Circuit of diagram of MMC; (b) Half-bridge module; (c) Full bridge module

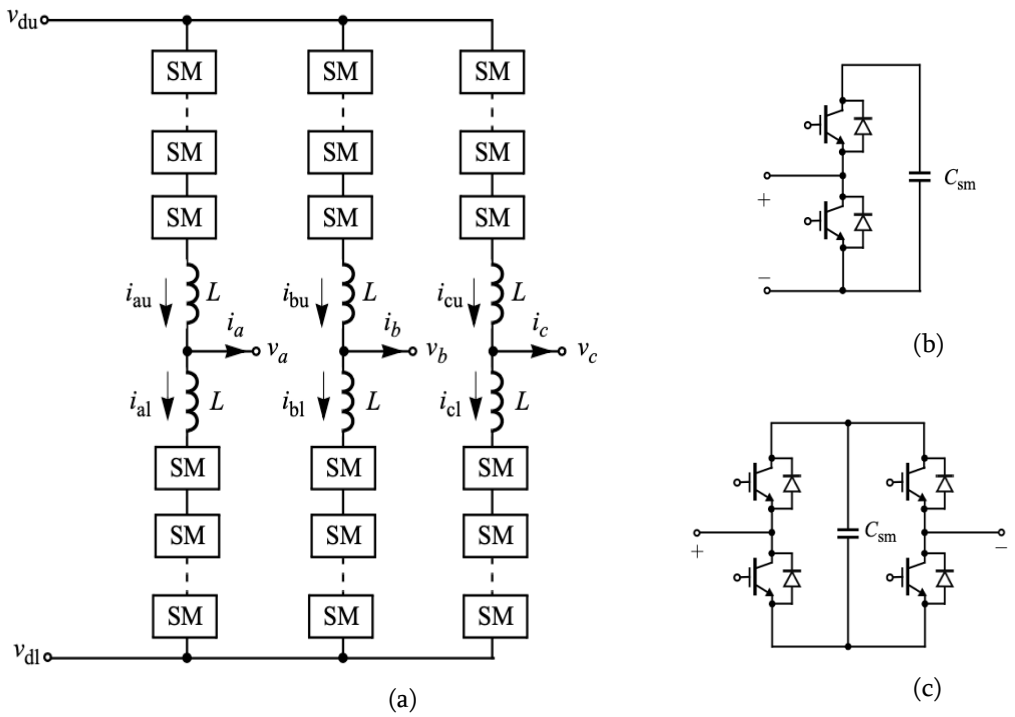

2.4 Advantages and Limitations of HVDC Architecture

Currently, most of the offshore wind farms under development in the US are being planned with MVAC collection system and HVAC transmission to onshore grids (except for Sunrise Wind) [12]. However, when the size of the wind farm and distance from the shore increase, the HVAC transmission becomes expensive and inefficient due to the cable costs and reactive power compensation. The HVDC

architecture overcomes these shortages with the dc transmission and leverages mature technologies of wind turbines (WT) and HVDC converters.

Although superior to HVAC transmission for longer distances, there are some limitations of the HVDC transmission. Within the offshore windfarms using HVDC architecture, there are multi-stage power conversions which could result in undesirable costs and losses. For example, in a typical offshore windfarm with HVDC transmission, the wind turbines output power at MVAC and 50/60Hz, the voltage is then stepped up to HVAC followed by conversion to HVDC by an offshore converter station; it is then transmitted via subsea cable and converted back to AC by an onshore converter station.

Another aspect of today's offshore wind farm design is that the electrical system within the WTs and transmission and distribution (T&D) architecture are separately designed (by different suppliers) leading to a lack of system level optimization. This approach results in a sub-optimal design of the power converters within the turbine and the transmission and distribution (T&D) infrastructure, leading to high electrical BOP costs and lower efficiency.

2.5 PSCAD Model of DC based Architecture

Like the model created for the AC architecture in Section 1.6, a PSCAD model for the HVDC architecture has been developed to perform engineering and tradeoff analyses. The one-line diagram of the PSCAD model is given in Figure 13.

Figure 13. PSCAD model of the wind farm for the HVDC architecture

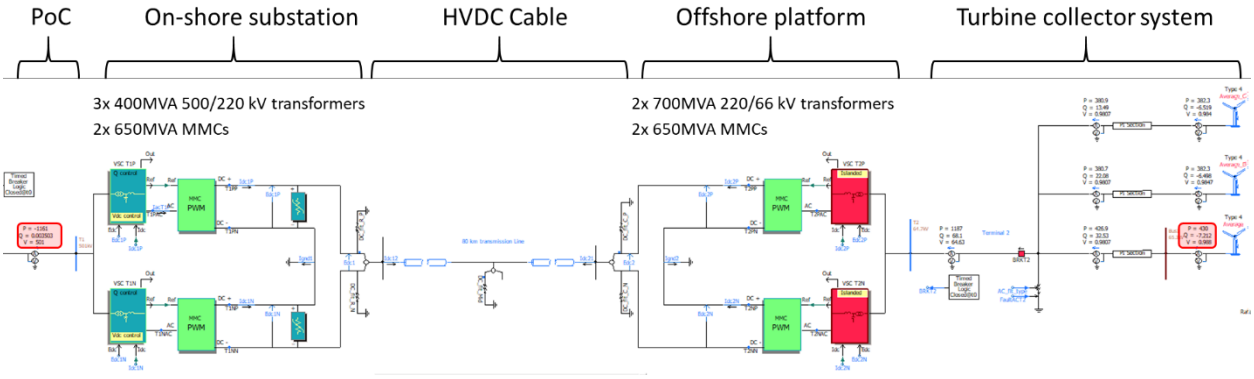

Starting from the right in Figure 13, the turbines are grouped into three aggregates similar to the model used in the HVAC wind farm architecture. The details of the turbine aggregation and wind turbine models are not repeated here since they are already given in Section 1.6. Instead of three offshore power transformers used in the HVAC design, two 700 MVA transformers serve as the converter step-up transformers in the HVDC design as given in Table 7. They step the voltage from 66 kV collector system

up to the 220 kV converter input. Unlike the HVAC design, no shunt reactors are needed since the MMC converters can absorb the collector cable charging current.

Two 80 km subsea HVDC transmission cables connect the offshore platform to the onshore MMCs. The parameters in Table 8 are entered into the frequency-dependent cable model in PSCAD to represent the HVDC cables. Neither shunt reactors nor a STATCOM is needed in the onshore substation for either compensating cable charging or reactive power injection requirements since a) DC transmission is used, and b) the converters can control their reactive power output. Lastly, three 400 MVA transformers step the voltage from 220 kV to 500 kV for utility interconnection. The point of connection busbar is labeled as “PoC”. The simulations of the same operating points as the ones given in Section 1.7 are presented in the next section to demonstrate compliance with the grid code requirements.

2.6 Simulation Results

In the HVDC architecture, the offshore system needs a 60 Hz AC voltage source for both energization and steady-state operation of the turbines. The offshore MMCs are configured in islanded mode to generate and maintain 60 Hz voltage for the collector system. Since the turbines can be considered as current sources injecting their output to the collector system, the offshore MMCs can then receive their injection as the voltage source of the offshore system. On the onshore side, the MMCs assume the DC bus control responsibility. With this arrangement, the whole system can seamlessly transfer the offshore wind generation through the DC cables to the onshore substation.

During energization of the wind farm, unlike the HVAC system, there are no overvoltage concerns as the offshore MMCs maintain the AC voltage for the collector system. The turbines are operated at unity power factor. On the onshore side, in addition to the DC bus regulation, MMCs can control their reactive power output. The plots below show simulation results for a 5 second simulation where the wind farm is energized and then ramped up to full output at 1,200 MW.

Figure 14. Real power output (MW) at the onshore PoC

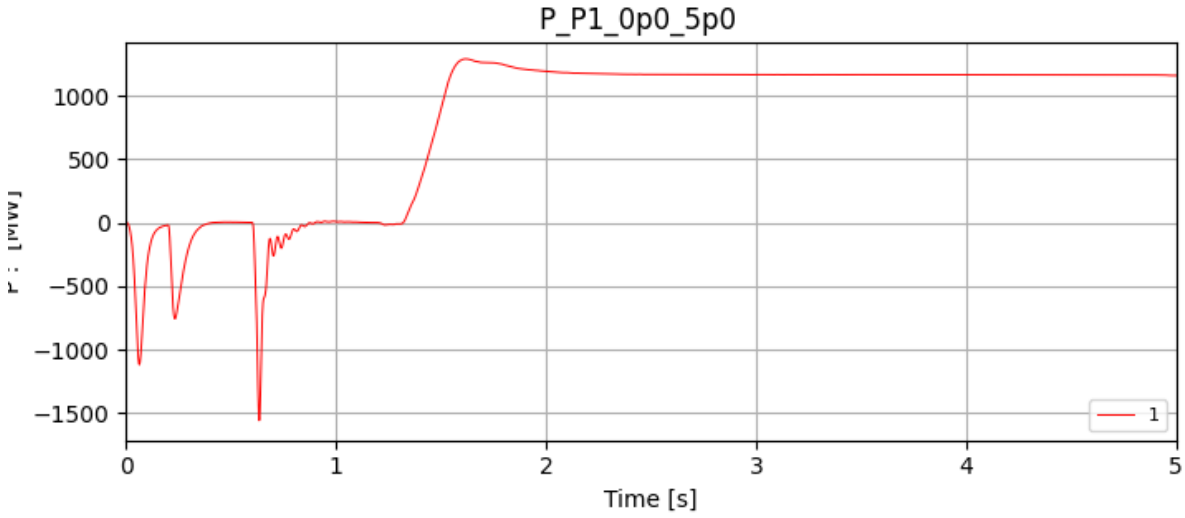

Figure 15. Real power injection (MW) into the offshore MMCs

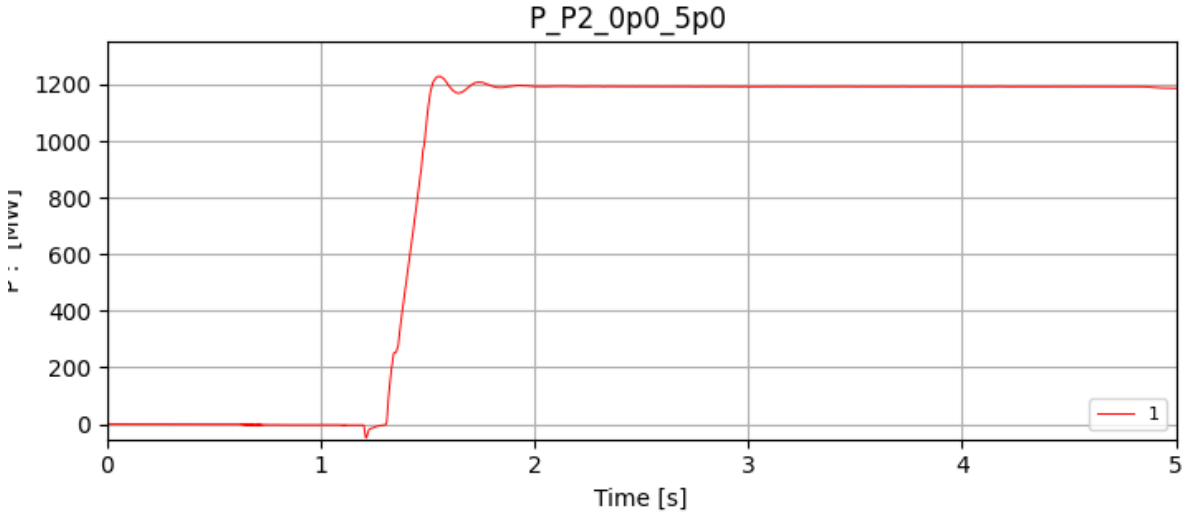

Figure 16. Reactive power injection (MVAR) into the offshore MMCs

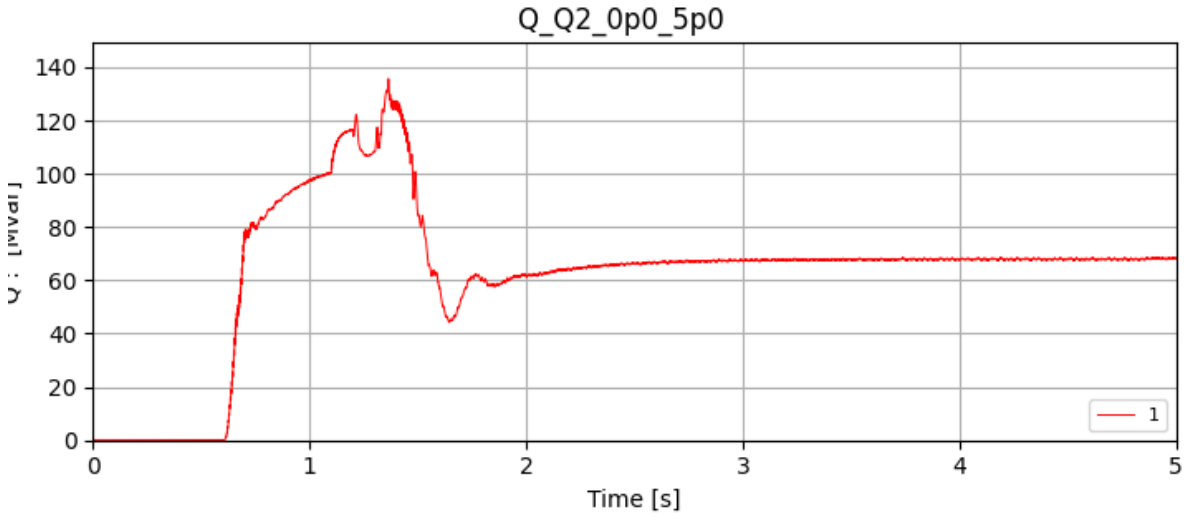

Figure 17. RMS voltage (kV) at the 66 kV side of the offshore MMCs

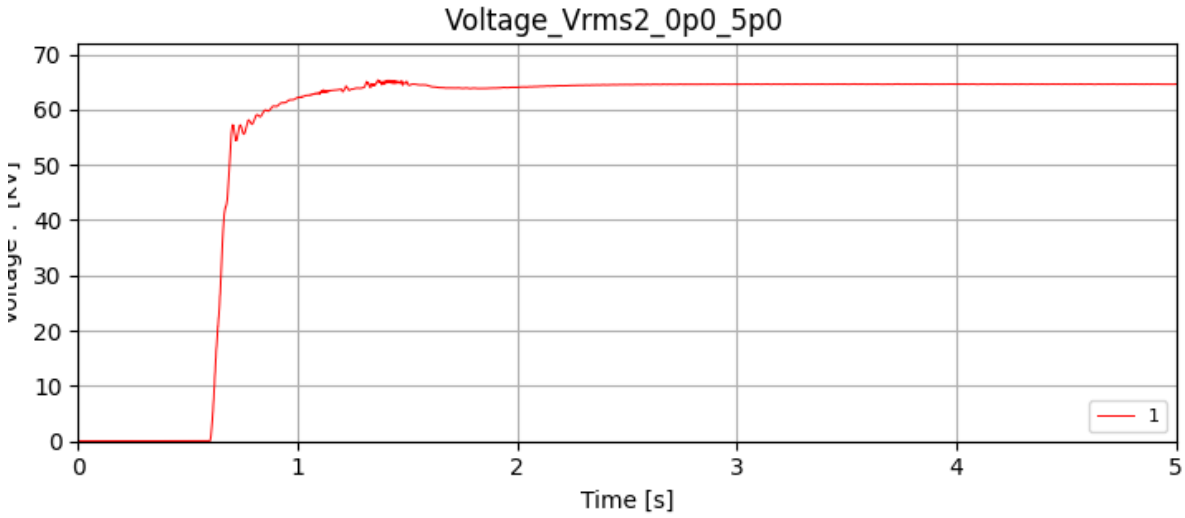

Figure 18. DC pole voltage (kV) for each pole of the bipolar system measured at the onshore side (A: 320 kV to ground, B: Ground to -320 kV)

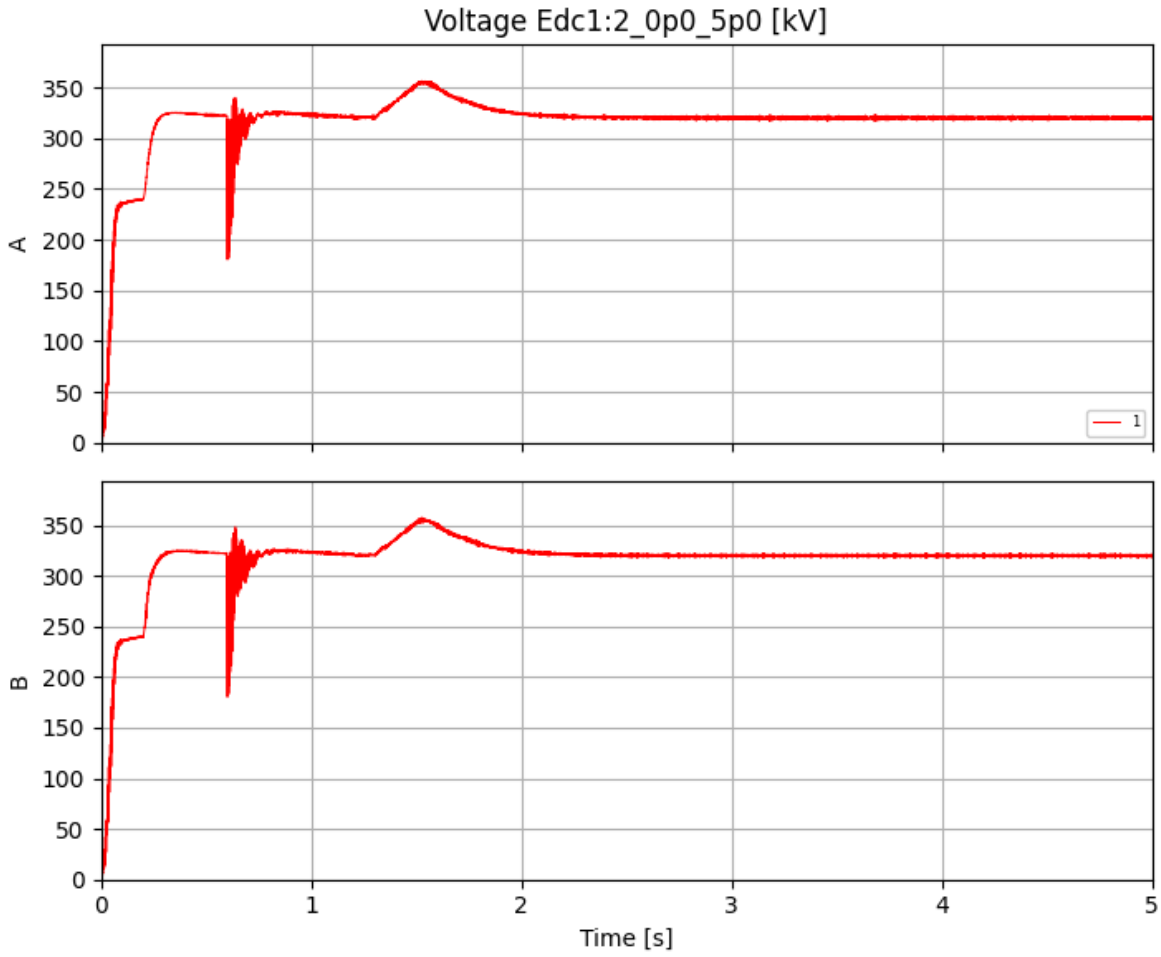

Figure 19. DC pole current (kA) measured injected at the offshore side (A: +320 kV, B: -320 kV)

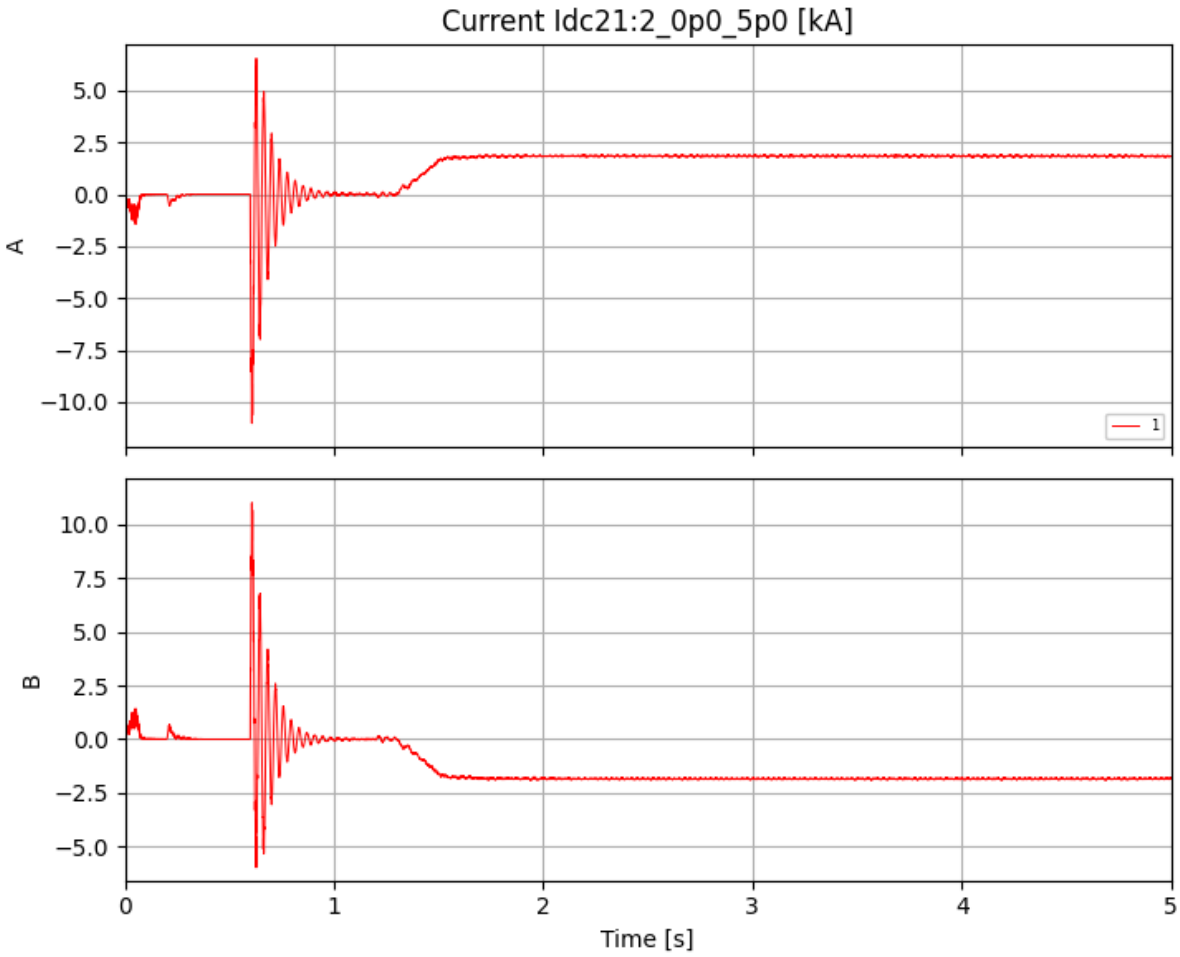

The four grid code requirement simulations given in Table 6 are repeated in the HVDC model to demonstrate compliance with the power factor requirements, which are described in Section 1.7.3. The results of the grid code simulations are given in Table 9 below.

Table 9. Grid Code Compliance Simulations for the HVDC System

Scenarios	Total Turbine P (MW)	Total Turbine Q[1] (MVAR)	Turb Term. Volt.[2] (pu)	Power Factor at the Turb. Term.	PoC P (MW)	PoC Q (MVAR)	PoC Power Factor	PoC Volt. (pu)	Reac. Power Def.[3] (MVAR)
Full output, 0.95 lagging PF	1200	-21	0.988	-1.000	1157	379	0.950	1.005	**Meets**
Full output, 0.95 leading PF	1200	-20	0.988	-1.000	1164	-377	-0.950	0.999	**Meets**
25% output, 0.95 lagging PF	307	8	0.983	1.000	297	378	0.950	1.004	**Meets**
25% output, 0.95 leading PF	307	9	0.983	1.000	305	-378	-0.950	0.997	**Meets**

[1]Although the turbines are set to operate at unity PF, there is small amount of loss through the scaling transformer used to aggregate the turbines.
[2]The highest terminal voltage of the three aggregated turbines is reported.
[3]Reactive power requirement is calculated for 1,150 MW injection regardless of the actual real power output. The PF requirement of 0.95 corresponds to +/- 378 MVAR reactive power delivered at the PoC.

The results in Table 9 cover two real power levels: full output and 25% output. For each power level, two reactive power setpoints are tested to see if the wind farm can meet the +/- 0.95 PF requirements, which correspond to +/- 378 MVAR reactive power delivered at the PoC for 1,150 MW net injection. The reason for using 1,150 MW injection for PF calculations is to keep the results aligned with the HVAC simulations given in Table 6. This comparison reveals that the HVAC solution has slightly higher real power losses than the HVDC solution.

In all simulations, the PoC voltage is maintained close to 1.0 pu. The voltage on the offshore side is maintained at 0.98 pu by the MMCs. The turbines operate at unity PF since their output is not relevant for voltage regulation at the PoC. As shown in Table 9, since all the reactive power requirements are met solely by the onshore MMCs, there is no need for shunt reactors or STATCOMs for grid code compliance.

2.7 Key Takeaways – HVDC Architecture

The VSC based HVDC topology utilizes mature technologies and has a growing install base around the world. It becomes cost effective compared with AC architecture for longer distances. The other advantages of the HVDC architecture over the HVAC architecture are:

1. Line cable charging current and the ensuing overvoltage issues are eliminated in the HVDC design.

2. The onshore MMCs have the capability to provide both leading and lagging reactive power similar to a large STATCOM. Therefore, all grid code requirements are met without any additional reactive power compensation devices.

In the next section, after developing the proposed MVDC architecture, some simulation results will be given to compare the wind farm's performance against the HVDC architecture.

3 Proposed MVDC Architecture

The proposed solution is shown in Figure 20 using the same 1.2 GW offshore wind farm example. Power from the offshore turbine (12 MW) will be generated at MVDC (~80 kVDC or other medium voltage level based on the techno-economic analysis). This is done through an isolated DC-DC step-up converter replacing the typical 60 Hz line side DC/AC converter. The isolation is provided through medium or high-frequency transformers (20 kHz-100 kHz instead of 60 Hz transformers). The overall cost of power electronics within the turbine remains largely unchanged; however, the benefit is in reducing the size and weight of the transformer by more than 50%. GE-R has developed this technology through several R&D projects from the Office of Naval Research (ONR), ARPA-e and DOE and can be adapted to large offshore wind converters. The MVDC outputs from several turbines are collected through an 80 kVDC cable and brought to an offshore platform. The outputs from several such groups form the inputs to the MVDC-HVDC converter.

3.1 Example with MVDC-HVDC Architecture

An example configuration is shown in Figure 20 consisting of 10 MVDC feeders connected to the bipolar MVDC/HVDC converter, 5 feeders on each side. 10 WTs are connected to each of the feeders. As a baseline, a DC-DC converter with MMC topology using series staked FB or HB SMs is considered. For the bipolar HVDC network, each string is configured in symmetric relation about an associated midpoint: the system ground. Each string comprises two pairs of arms; each pair of arms consisting of an inner arm (with HB SMs) and an outer arm (with FB SMs): an arm being a set of cascaded SMs. The ratio of FB and HB SMs is dependent on the voltage gain required for MVDC-HVDC conversion. The converter has bidirectional power flow capability and with the use of FB sub-modules in the circuit, fault currents on the input or output sides can be blocked. The MVDC collection feeder voltage is considered as 80 kV for now; however, the optimal voltage will be obtained from the systems study. The MVDC-HVDC converter converts 80 kV to 320 kV for transmission by subsea cable in a bipolar configuration. In the onshore substation, HVDC is converted back to 345 kV AC. Similar to the previous cases, the onshore substation has three 345 kV/ 500 kV/ 13.8 kV 400 MVA transformer, associated disconnects, CBs, and control and protection platforms to connect to the grid.

Figure 20. Example of MVDC collection, HVDC transmission system

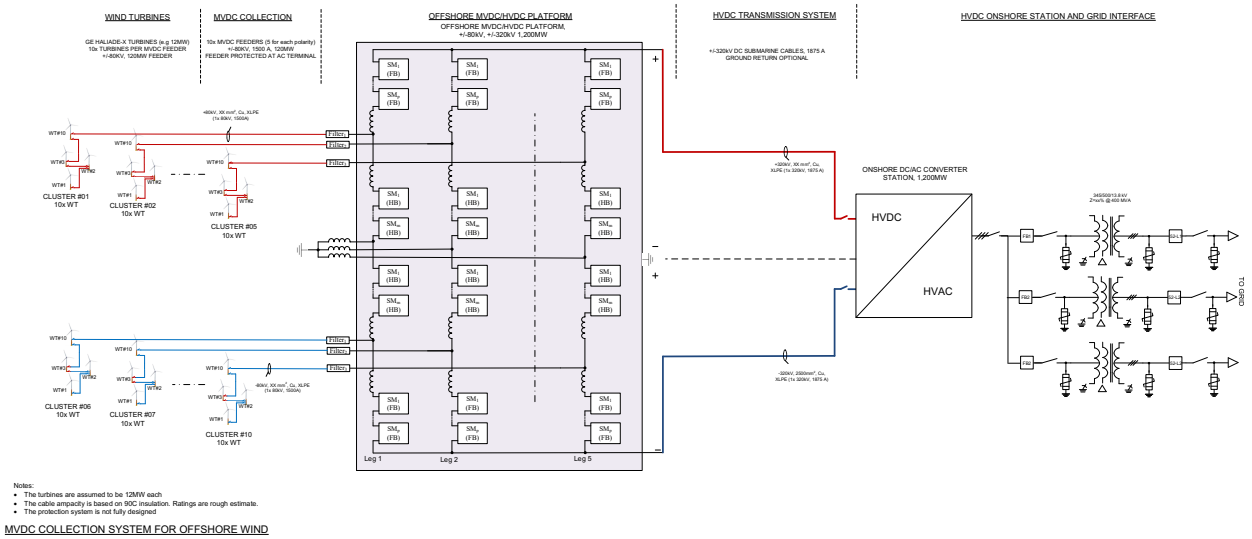

3.2 Converter Technology Options for MVDC-HVDC

The MVDC-HVDC power conversion needs to handle high voltage (>300 kV) and current (>2 kA), which makes the modular dc/dc converter design attractive as it can reduce the requirement for high-voltage and high-current switches as well as bulky passive components such as filter inductors and capacitors [13]. By connecting the ac terminal of two MMC-HVDC converter together through an ac transformer as shown in Figure 21**Error! Reference source not found.**(a), the MVDC-HVDC power conversion with galvanic isolation can be achieved through a three-stage dc-ac-dc conversion.

Figure 21. Example of MVDC collection, HVDC transmission system

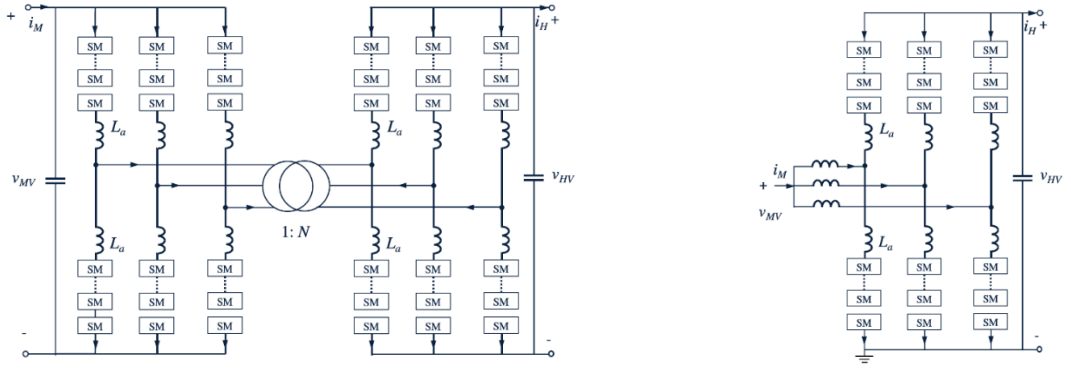

(a) Isolated MMC dc-dc converter (b) Non-Isolated MMC dc-dc converter

However, the use of the ac transformer and two MMC converters will increase the footprint of converter station and increase system losses. Therefore, it will not be a preferred solution for offshore wind farm applications. An alternative is to directly connect the ac terminal of one MMC with filters to form the MVDC terminal, as shown in Figure 21(b). In this topology, the power conversion will be based on the dc and ac currents flowing through the converter arms and will leverage the existing converter architecture where the same SMs in MMC-HVDC can be used. In addition, if FB SMs are used in the upper arms, the converter will be able to provide dc fault blocking capability [14] which is critical the offshore wind farms.

Another possible MVDC-HVDC converter topology is based on switched capacitor (SC) converters as shown in Figure 22 [15]. In this topology, the capacitors of the cells will switch between two states of connections (taking the cell 1 to 3 of positive rail as an example): a) when green switches are on and red switches are off, capacitors Cr are connected in parallel to MV side b) when green switches are off and red switches are on, capacitors Cr are connected in series to charge the HV side capacitor and load. In this topology, the fault current blocking capability can also be achieved with additional control current circuit [15].

Figure 22. Circuit diagram of switched capacitor-base MVDC-HVDC converter [15].

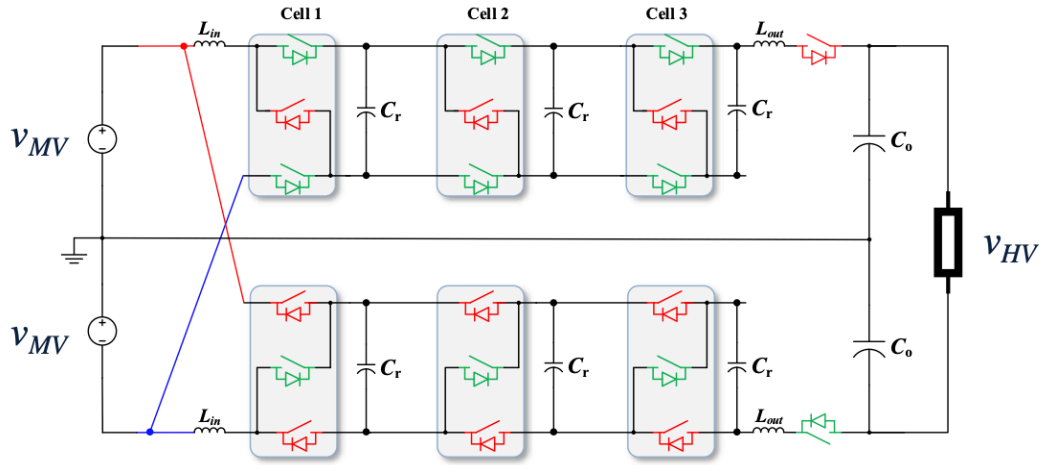

Currently the converters presented in Figure 21(b) are being investigated to understand its operation principles and constrains with preliminary steady-state analysis and PSCAD simulations.

3.3 Converter Model and Simulations: MMC-based DC-DC

In Figure 23, an equivalent circuit of the MMC-based DC-DC converter Figure 21(b) is derived for one single phase leg. In the equivalent circuit, the inserted voltages of the upper and lower arms are v_u and v_l,

respectively. i_u and i_l are the currents of upper and lower arms; i_H and v_H are current and voltage of the HVDC terminals, respectively; and i_M and v_M are current and voltage of MVDC terminals, respectively. To simplify the steady-state operation analysis, the following assumptions are made [14]:

1) Continuous voltages (v_u and v_l) are synthesized with inserted SMs.
2) Arm voltages and currents contain only steady-state fundamental frequency and dc components.
3) Resistance and switching losses are neglected.
4) Input and output currents i_M and i_H are harmonic free and contain DC only; harmonics currents will only circulate within phases.

Figure 23. Equivalent circuit diagram of a single phase in MMC.

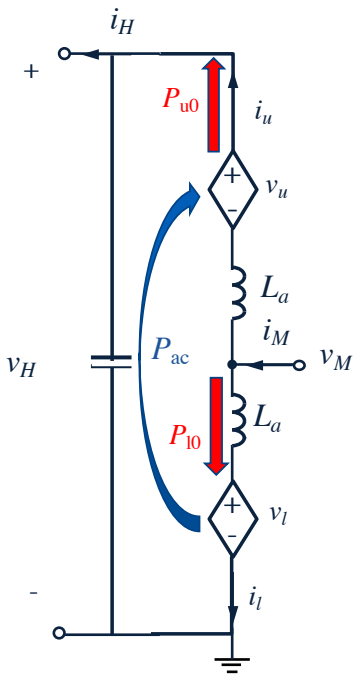

Therefore, the arm currents and voltages can be written as,

$$v_u = V_{u0} + V_{u1}\cos(w_1 t + q_{vu}),\ \ i_u = I_{u0} + I_{u1}\cos(w_1 t + q_{iu})$$

$$v_l = V_{l0} + V_{l1}\cos(w_1 t + q_{vl}),\ \ i_l = I_{l0} + I_{l1}\cos(w_1 t + q_{il})$$

where V_{u0} and are V_{l0} are the inserted DC voltages of the upper and lower arms; I_{u0} and I_{l0} are the DC currents of the upper and lower arms; V_{u1} and V_{l1} are the inserted AC voltages of the upper and lower arms; I_{u1} and are I_{l1} are the AC currents of upper and lower arms. Note that high order harmonics are not considered in the steady-state analysis. Assuming the voltage ratio between HV and MV terminals is D, and I_H and V_H are the DC current and voltage respectively, then the relationship between the DC operating points can be written as below.

$$D = v_M/v_H,\ V_{l0} / V_{u0} = D/(1\text{-}D)\ \ i_H = I_H,\ \ i_M = I_H /D$$

The upper arm dc current and voltage as well as dc power output can be written as:

$$I_{u0} = I_H,\ V_{u0} = (1\text{-}D)\ V_H,\ P_{u0} = V_H I_H\ (1\text{-}D).$$

The lower arm dc current and voltage as well as dc power output can be written as:

$$I_{l0} = I_H\ (1\text{-}D)/D,\ V_{l0} = DV_H,\ P_{l0} = V_H\ I_H(D\text{-}1).$$

Note that P_{l0} is defined as the power output of the arm capacitors so $P_{l0} = -I_{l0}\ V_{l0}$. The DC power output P_{u0} and P_{l0} are shown in Figure 23: when the power flows from MVDC to HVDC terminal, the upper arm capacitors are outputting DC power P_{u0} while the lower arm capacitors are absorbing the DC power P_{l0}. Without additional power flow, the energy of the upper and low arms will become unbalanced. Therefore, it is necessary to make the AC power P_{ac} circulate between the upper and lower arms to maintain proper voltage level of the arm capacitors. The power exchange due to the AC component, P_{ac}, can be calculated as

$$P_{ac} = \frac{\sin(q_{vu} - q_{vl})\ V_{l1}\ V_{u1}}{4X_{la}}$$

where X_{la} represents the impedance of the arm inductor at the AC frequency. In steady-state operation, the DC and AC power exchange should be balanced $P_{ac} = P_{u0} = -P_{l0}$. The above equations explain the fundamental principles of the converter operation.

To validate the operation of the MMC-based MVDC-HVDC converter as shown in Figure 21 (b), a simple open-loop control circuit is simulated in PSCAD. The step-up ratio is set to be 1:2 (300 kV:600 kV) and there are 76 SMs in each arm. The simulation circuit is shown in Figure 24. Note that this example does not reflect the final design of the MVDC-HVDC converter, instead it is used as an example case to demonstrate the operation.

Figure 24. Equivalent circuit diagram of a single phase in MMC.

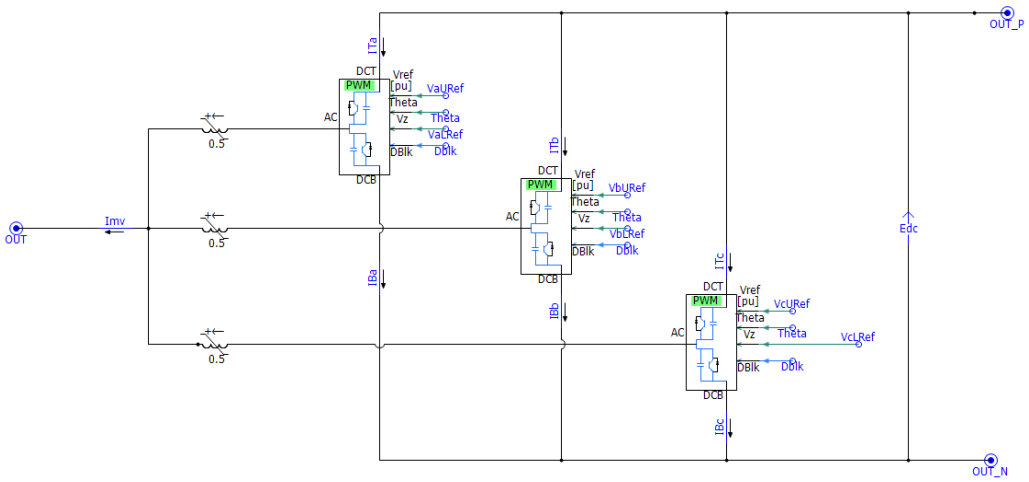

Figure 25 and Figure 26 show the simulated responses of the arm capacitor voltages and inductor currents: The upper traces in Figure 25 show the sum of the upper and lower arm capacitor voltages within one phase leg and the lower traces show the maximum capacitor voltages of the SMs. From Figure 25, it is seen that the sum of the arm capacitor voltages is well balanced between the upper and lower arms. The capacitor voltage of 400 kV represents 75% voltage utilization of the arm volage (300 kV/ 400 kV). This ratio can be further optimized through control improvement.

Figure 25. Upper and lower arm capacitor voltage responses of one phase.

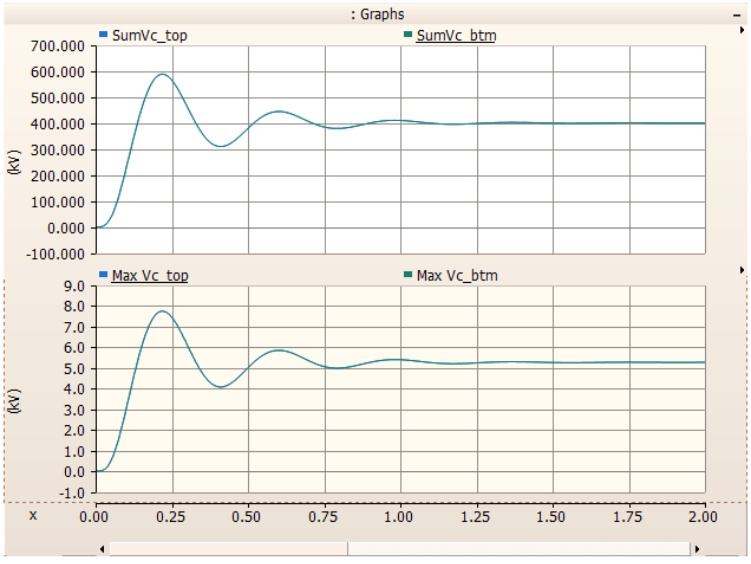

Figure 26 shows the currents of the upper arms of the three-phase legs; it can be observed that these currents contain both DC component and AC harmonics. In the conventional MMC-HVDC converter where output voltage and current are AC components (at fundamental frequency) at its AC terminals, the DC currents will circulate between upper and lower arms to balance the arm energy. In the MVDC-HVDC converter, as explained above, the input and output terminal currents will be DC, but AC currents will circulate within the phase legs to exchange power between the upper and lower arms in order to balance the arm capacitor energy.

Figure 26. Three phase legs upper arm current responses.

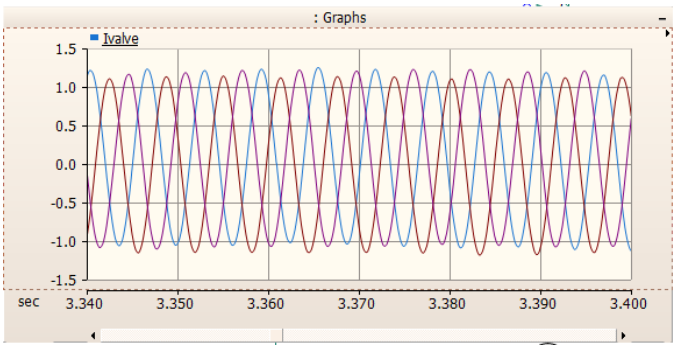

3.4 Converter Model and Simulations: SC-based DC-DC

In this section, the simulation model and results of the SC-based DC-DC converter as shown in Figure 22 are presented. The voltage stress of each of the intermediate capacitor Cr is twice the input voltage, $V_{Cr} = 2V_{MV}$, while the output voltage is a function of the input voltage and the number of stages, $V_{HV} = (2n+1)V_{MV}$, where n is the number of stages. Each stage or cell module is characterized by three switching devices (Sw1, Sw2, Sw3) and a switched capacitor (Cr) as shown in Figure 27. The voltage and current stress for each of these cell modules is dependent on the relative position of the cell module in the converter. And based on the voltage and current of the cell module, the number of IGBT modules to be connected in series/parallel for each of these three switches will be determined. Though the operation of this converter is straightforward, one limitation of this converter is the capability to control the output voltage. As the gain of this converter is discrete and depends on the number of stages [$V_{HV} = (2n+1)V_{MV}$], it is fixed at the design stage and cannot be controlled with conventional pulse width modulation technique (PWM) used in standard DC-DC converter.

Figure 27. Each module cell of SC-based converter

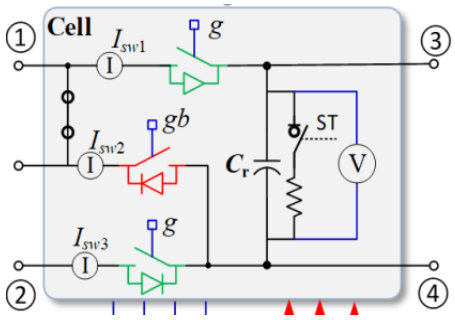

For this study, the converter is considered for three different medium voltage levels: input voltage of 46 kV, 64 kV and 107 kV as shown in Figure 28, Figure 29 and Figure 30 respectively, with 320 kV on the HV side for each pole to ground. Based on the voltage gain requirement, these need 3-stage, 2-stage, or 1-stage implementation respectively as shown.

Figure 28. 3-stage converter for 46 kV MVDC voltage

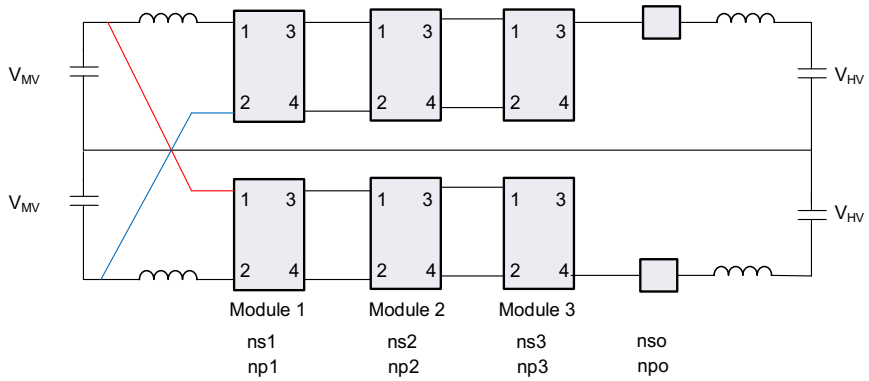

Figure 29. 2-stage converter for 64 kV MVDC voltage

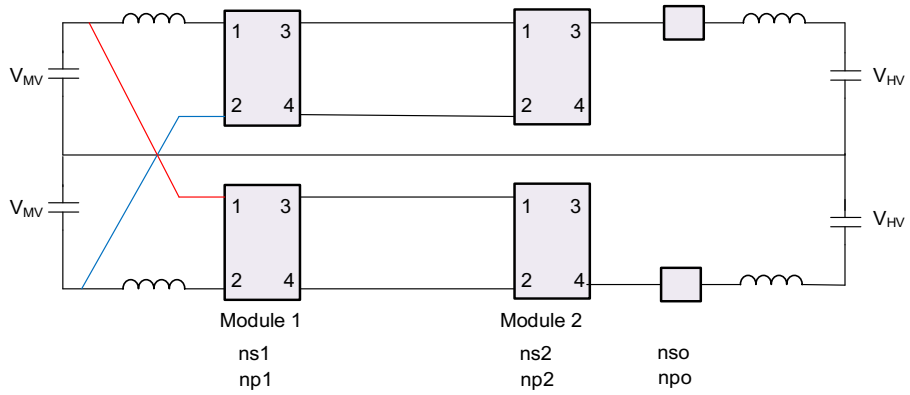

Figure 30.-stage converter for 107 kV MVDC voltage

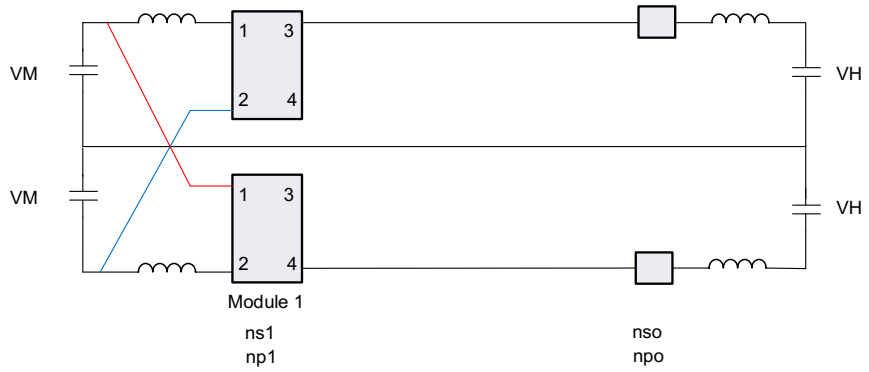

As mentioned, the voltage and current stress for each of these cell modules is dependent on the relative position of the cell in the converter. So, the number of IGBT modules required to be in series and parallel for each switch (Sw1, Sw2, or Sw3) in a cell is not same for all the implementations. However, it is fixed for all the switches in a particular cell module. In Figure 28, ns1 and np1 represents the number of IGBT modules to be connected in series and parallel respectively for each switch in cell module 1. Similar representation is followed for other cell modules as well in Figure 28, Figure 29 and Figure 30. While nso and npo represents the number of IGBT modules to be connected in series and parallel respectively for the output switch. An example of the number of IGBT modules required for the full converter is included in the next Sub section 3.5.

To verify the converter's operation, one pole of the bipolar structure is simulated in PSCAD for the rated power (600 MVA for each pole, 1.2 GW for the farm) for 3-stage operation with 46 kV MVDC input voltage. PSCAD simulation model of the single pole converter operating in open loop is shown in Figure 31.. The input inductors and cell capacitors are selected based on the soft switching operation of the switches [15]. Figure 32 shows the simulation results of single pole converter with 3-stage showing output and intermediate capacitor voltages (a), input (b) and output (c) current. As expected, the capacitor voltage is 92 kV which is twice the MVDC input voltage, and output is 320 kV which is 7 times the input voltage. The input current shown in Figure 32 (b) has switching frequency ripple. The output current ripple is shown in Figure 32 (c) along with its RMS value.

Figure 31. PSCAD model for the 3-stage SC based DC-DC converter

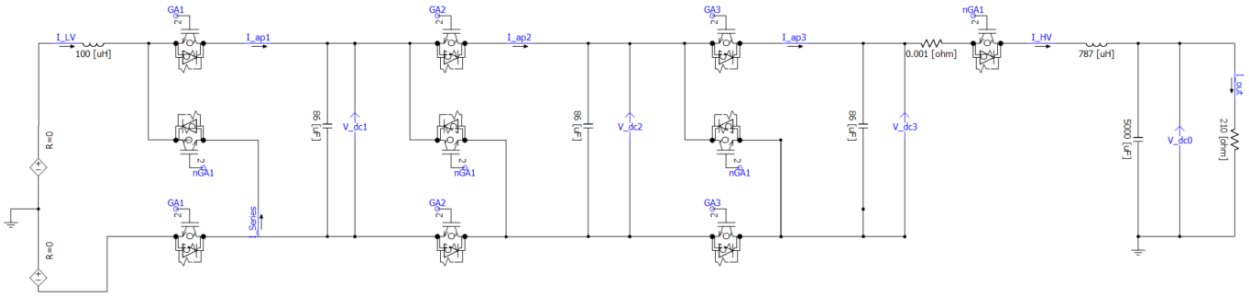

Figure 32. Simulation results of single pole 3-stage converter for 46 kV input and 320 kV output at 600 MW showing output and intermediate capacitor voltages (a), input (b) and output (c) current.

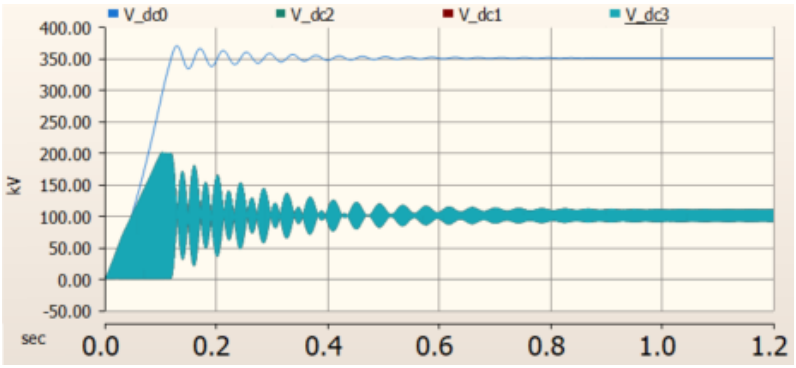

(a)

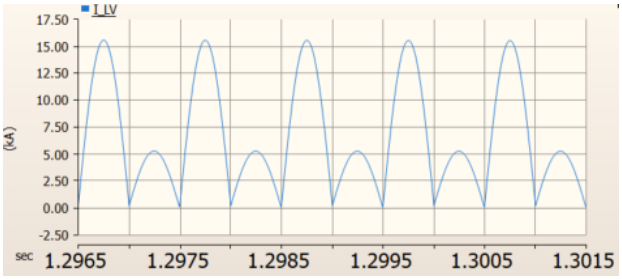

(b)

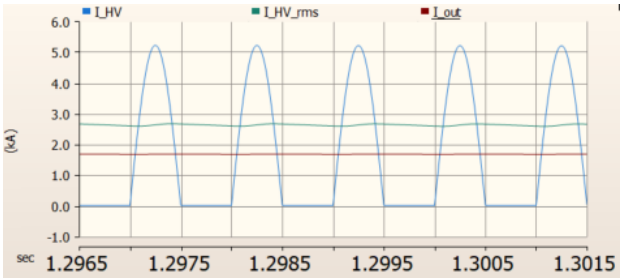

(c)

3.5 Comparison of number of IGBT modules required for different configurations

The cost of the power electronics is primarily guided by the cost of the switching devices: IGBT modules. The number of the IGBT modules for both the MMC DC-DC and SC DC-DC is compared for different input medium voltages. As noted in previous Section 3.3, the operating principles of MMC DC-DC require superimposition of an AC component in the upper and lower arm voltage. And this voltage is a

function of the converter gain: higher the gain required, higher is the AC voltage requiring a lot more SMs to be series connected, making this converter less attractive from the cost viewpoint. Figure 33 **(a)** shows the number of HB and FB SM required for 1.2 GW windfarm example considered here. Figure 33 **(b)** gives the corresponding total number of IGBT modules required for different V_{MV}. Please note that the FB SMs are required in the upper arm to ensure fault blocking capability in either side of the converter. The number of modules to be paralleled, i.e., the number of MMC arms in each pole depends on the rated current. In the example, each of the SMs is considered to be rated for 4.6 kV, 1.6 kA. Even without derating and not considering for redundancy, the number of FB and HB required at V_{MV}= 65 kV are 88 and 21 respectively which account to 11,100 IGBT modules for 14 MMC arms. This number is very high in comparison to the traditional DC-AC MMC.

Figure 33. SMs (HB and FB), IGBT modules for MMC DC-DC converter for different input MV

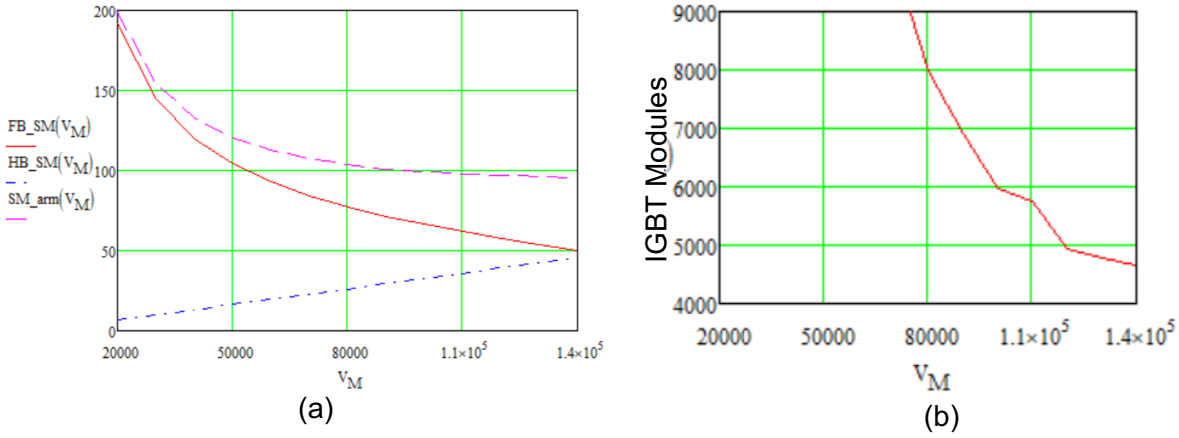

In contrast, the number of IGBT modules required for the SC DC-DC converter is comparable to that of conventional AC MMC. Table 10 shows the number of IGBT modules required for 3 different V_{MV} cases as described in Section 3.4. The number of IGBT modules to be connected in series and parallel (ns, np) for each cell module as well as for the output switch (nso, npo) are given for each of the cases. Finally, the last column gives the total IGBT modules required for 2 poles. It is to be noted that the total IGBT modules for each cell module is given by thrice the product of number of IGBT modules in series and number of them in parallel. For e.g., for cell module 1, the total IGBT module in cell module 1 for each pole = 3*ns1*np1. From the Table 10, for case 1, it is 3*26*15 = 1170 for each pole. The factor of 3 comes because each cell module constitutes of 3 switches.

The calculation in this Table 10 considers IGBT module rated at 6.5 kV, 1000 A, and derated to 3.6 kV, 800 A considering factor of safety and redundancy. The number of IGBT modules required in a conventional DC-AC MMC (HB SMs designed with similar redundancy) is around 4600. Comparing it

with the SC-based converter, it can be seen that the number of IGBT modules are comparable for MVDC voltage of 64 kV and has been considered for the cost estimates in the next Section 4.

Table 10 Number of IGBT modules required for SC DC-DC converter

Medium voltage	Cell Module 1 for each pole	Cell Module 2 for each pole	Cell Module 3 for each pole	Output device for each pole	Total IGBT modules for 2 poles
V_{MV} = 46 kV	ns1 = 26 np1 = 15	ns2 = 26 np2 = 10	ns3 = 26 np3 = 5	nso = 89 npo = 5	5570
V_{MV} = 64 kV	ns1 = 36 np1 = 10	ns2 = 36 np2 = 5	NA	nso = 89 npo = 5	4130
V_{MV} = 107 kV	ns1 = 59 np1 = 5	NA	NA	nso = 89 npo = 5	2660

3.6 PSCAD Model for Offshore Wind Farm with SC MVDC-HVDC Architecture

The proposed switched capacitor MVDC-HVDC dc-dc converter is integrated into the offshore wind farm model developed in the section 2.5. In the PSCAD model as shown in Figure 34, the onshore MMC-HVDC inverter and HVDC cables remain the same, and the HVDC voltage level is ±320 kV as well. However, the offshore HVDC rectifier is replaced by the bipolar SC dc-dc converter with ±46 kV MVDC input. The wind turbines are modified to output ±46 kV MVDC voltage with medium voltage (MV) step-up transformers and six-pulse diode rectifiers. Note that the wind turbine MV step-up transformers in this case can be a medium frequency (up to several hundred Hertz) transformer to further reduce their size and weight. The wind turbine grid side inverter control is modified with fixed out ac frequency and eliminating the phase lock loop (PLL). To reduce the computational complexity of the PSCAD model and reduce simulation time, the wind turbines are lumped into two identical units of which the generators and the generator converters are simplified into ideal current source. The simulation results are shown in Figure 35 and it proves that proposed architecture can be stable in steady-state operation.

Figure 34. PSCAD Model for offshore wind farm with SC MVDC-HVDC architecture.

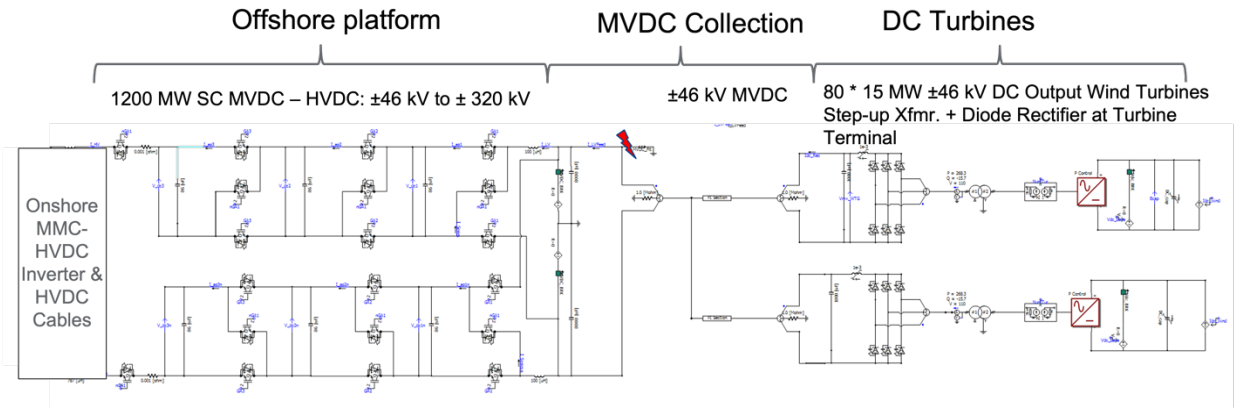

Figure 35. PSCAD simulation of offshore wind farm with SC MVDC-HVDC architecture.

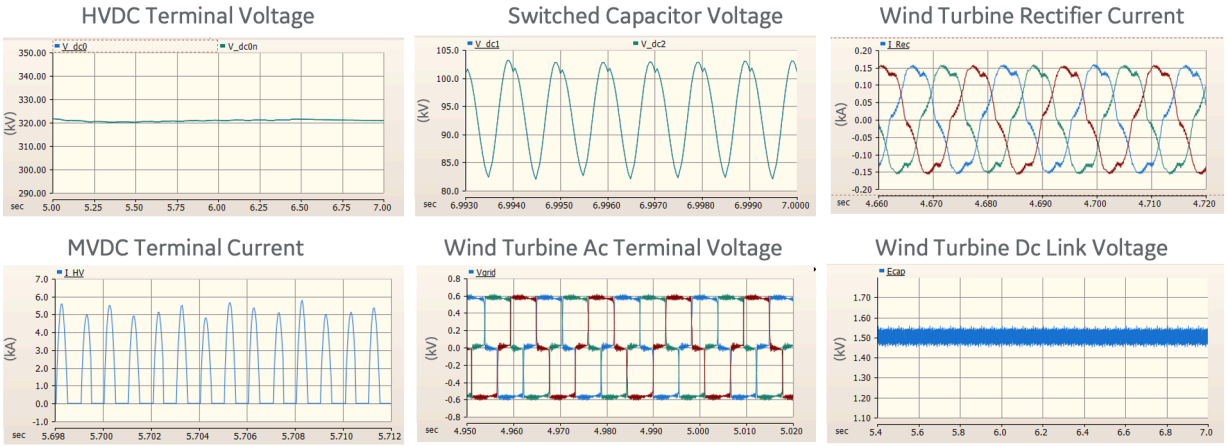

In addition to the steady-state operation, the fault behavior of the MVDC collection system is also studied. The line to ground fault at the MVDC feeder (as highlighted by the red arrow in Figure 34) is simulated and analyzed. In the fault simulation, the protection such as dc circuit breaker is not considered. MVDC terminal line-to-ground fault is the fault between positive or negative pole of MVDC terminal and ground. In this report positive pole fault is simulated as shown in Figure 34. Figure 36 shows the simulated responses. The system is running at the rated power before the fault and at 6s (t0) the line-to-ground fault is applied with 1ohm fault impedance.

In Figure 36, from t0 to t1, the voltage of the positive pole of MVDC terminal (V_dcMV_P) will drop quickly due to discharging of the capacitor as the fault current (IFlt_MVDC) steps up. This fault current is mainly from the discharge of MVDC capacitor and cable capacitance. Due to ungrounded connection of the wind turbine diode rectifier, wind turbine hardly contributes to the ground fault current during this period. Meanwhile, the voltage of the negative pole of MVDC terminal (V_dcMV_N) increases quickly

due to the redistribution of the energy at MVDC link. Also, because of the loss of positive pole voltage at the MVDC terminal, the direction SC converter input and output current (I_LV and I_HV) is reversed because the sum of the voltages of the switched capacitors are less than the voltage of the positive pole of HVDC link (V_dc0).

From t1 to t2, MVDC terminal positive pole volage (V_dcMV_P) drops slows due to the fault discharging and the fault current remains low. The voltage of the SC capacitor voltage are gradually increasing (V_dcMV, which is the sum of V_dcMV_P and V_dcMV_N). The direction SC converter input and output current (I_LV and I_HV) is still reversed compared to normal operation until t2.

From t_2, the direction SC converter input and output current (I_LV and I_HV) return to normal operation condition. Due to the line-to-ground fault at positive pole and energy redistribution to the negative pole capacitor which essentially reduces the MVDC link capacitance, the MVDC voltage (V_dcMV) increases beyond 2*46kV. Also, the unbalanced MVDC voltage leads to the unbalanced HVDC voltage.

From the simulation results, the line to ground fault at MVDC terminal create less current stress to converters if the wind turbine diode rectifier is not grounded. However, unbalanced fault will create unbalanced voltages at both MVDC and HVDC terminal. These unbalanced voltages result in the overvoltage of the dc capacitance and bring additional voltage stress to the components.

In Figure 37, the steady-state responses of the line to ground fault at the MVDC link are plotted. Due to the loss of MVDC positive pole, the steady-state voltage conversion ratio is changed: at the positive pole the HVDC voltage (V_dc0) will be three times of MVDC voltage (Vdc_MV) and at the negative pole the HVDC voltage (V_dc0n) will be four times of the MVDC voltage (Vdc_MV). From the simulation results, steady-state value of V_dc0 is around 320 kV, V_dc0n is 428 kV and Vdc_MV is 107 kV. And in fault steady state, the HVDC positive pole voltage will still be regulated by onshore inverter at 320 kV while the HVDC negative pole voltage will be clamped by the switched capacitors. From Figure 37, it can be observed that the line to ground fault will lead to unbalanced pole voltage as well as overvoltage at both MVDC and HVDC links. To maintain the continuous operation under such fault condition, the healthy MVDC pole with have an overvoltage of 232% and the healthy HVDC pole will have an over voltage of 134%. In addition, due to the unbalanced operation, significant ground current will flow through the HVDC link grounding point.

Figure 36. PSCAD simulation of MVDC terminal line to ground fault

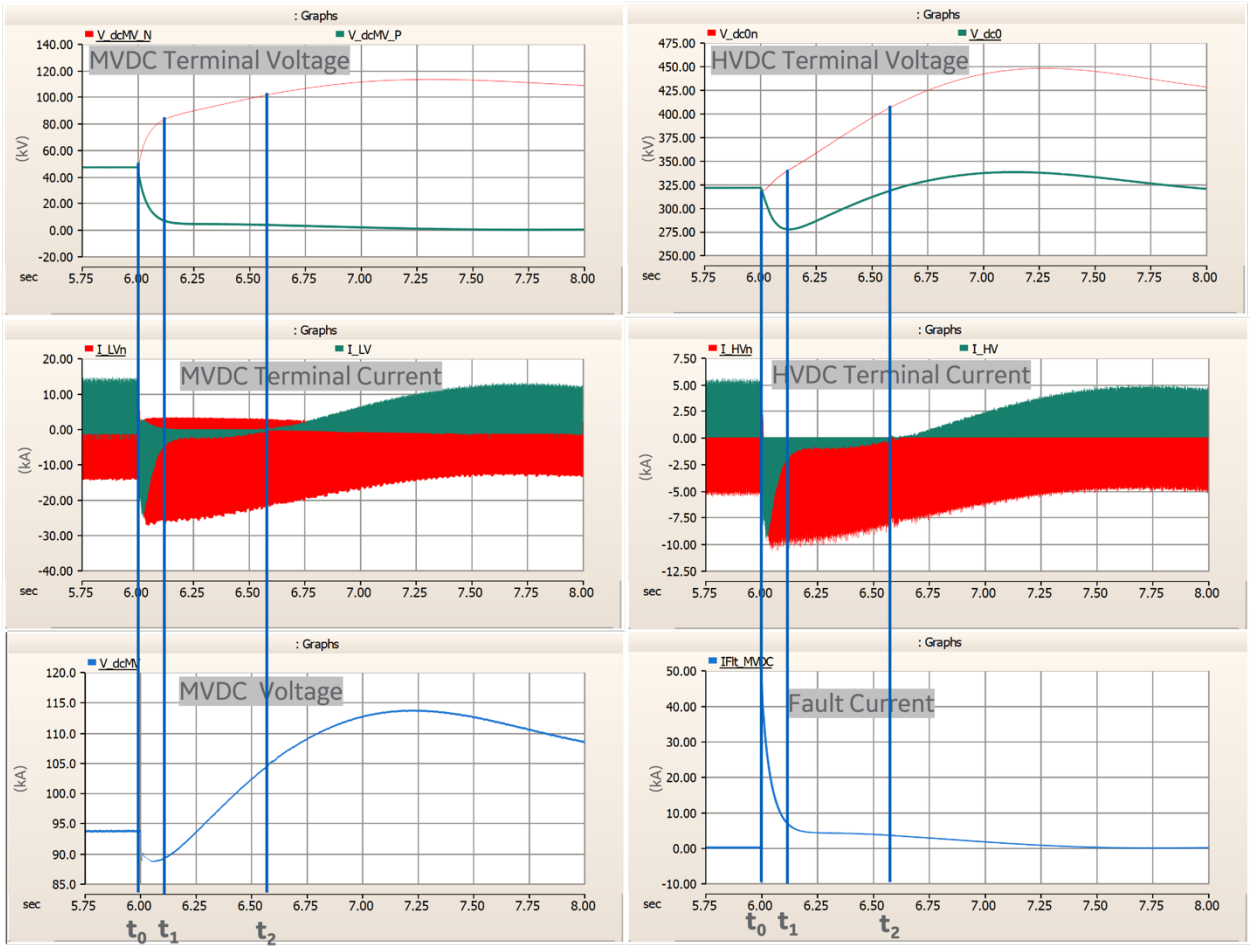

Figure 37. PSCAD simulation of MVDC terminal line to ground fault – stead state.

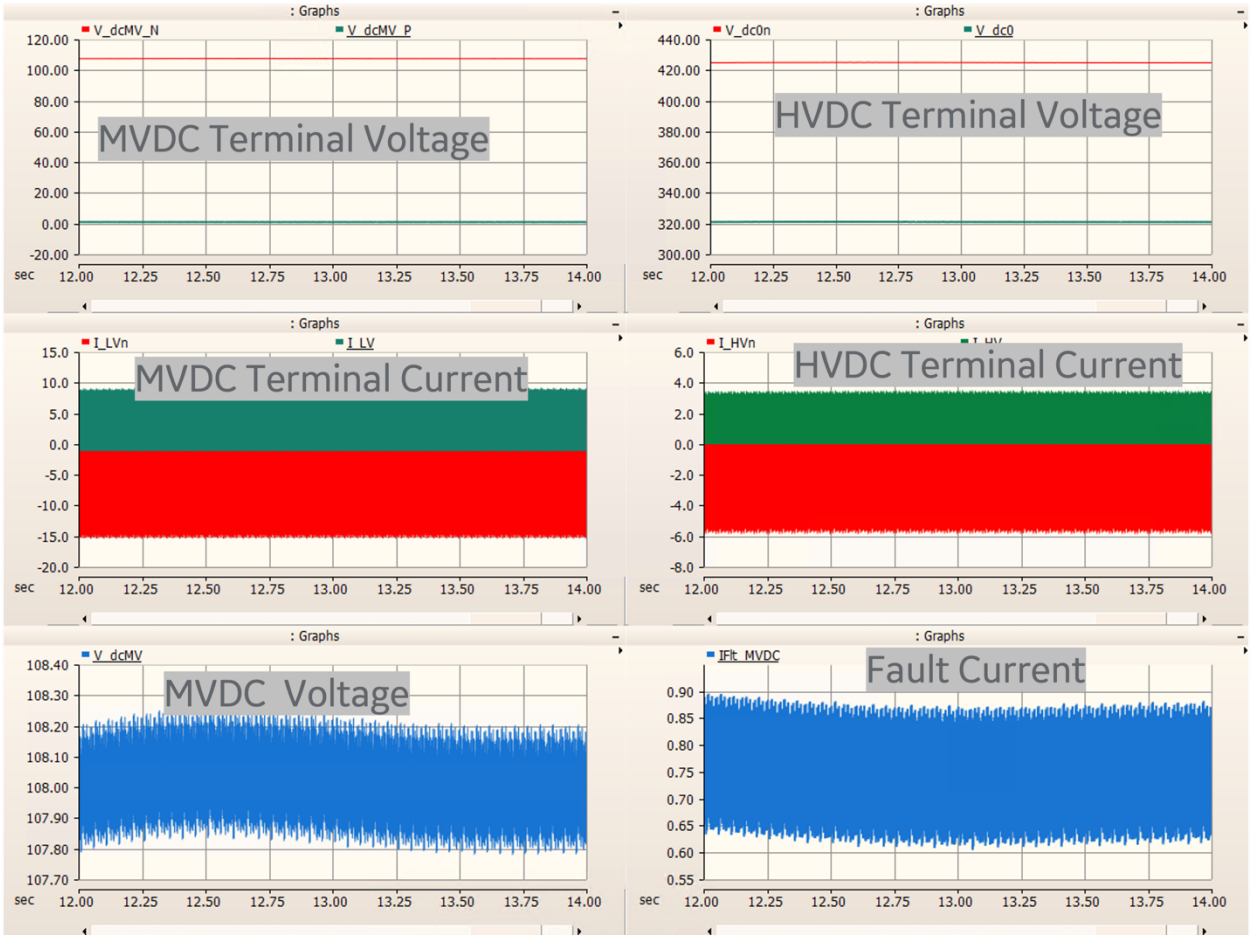

Assume that the unbalanced MVDC voltage can be quickly detected by the wind turbines through measuring the pole to ground voltages at their MVDC output terminals, wind turbines can be quickly tripped to protect the MVDC-HVDC converter. Figure 38 shows the simulation results of tripping wind turbines 10ms after the fault occurred. It can be observed that the healthy MVDC pole voltage (Vdc_MV_N) quickly ramped up from 46 kV to more than 80kV due to unbalanced fault. The voltage of negative pole of HVDC link slightly overshot to 330 kV and then returned to rated 320 kV under onshore inverter control and this clamped MVDC voltage to around 80 kV and the voltage of positive pole of HVDC link was clamped by the MVDC voltage at around 270 kV and the onshore inverter lost the control of the HVDC link voltage at its positive pole. Note that the current also circulated from the positive pole (faulted) to negative pole(healthy) with the MVDC link. The fast trip can help to mitigate

the overvoltage at the HVDC link but cannot avoid the overvoltage at the MVDC link. In addition, it can also cause undervoltage the at HVDC link which will affect the control of the onshore inverter.

Figure 38. PSCAD simulation of MVDC terminal line to ground fault – fast tripping of wind turbines.

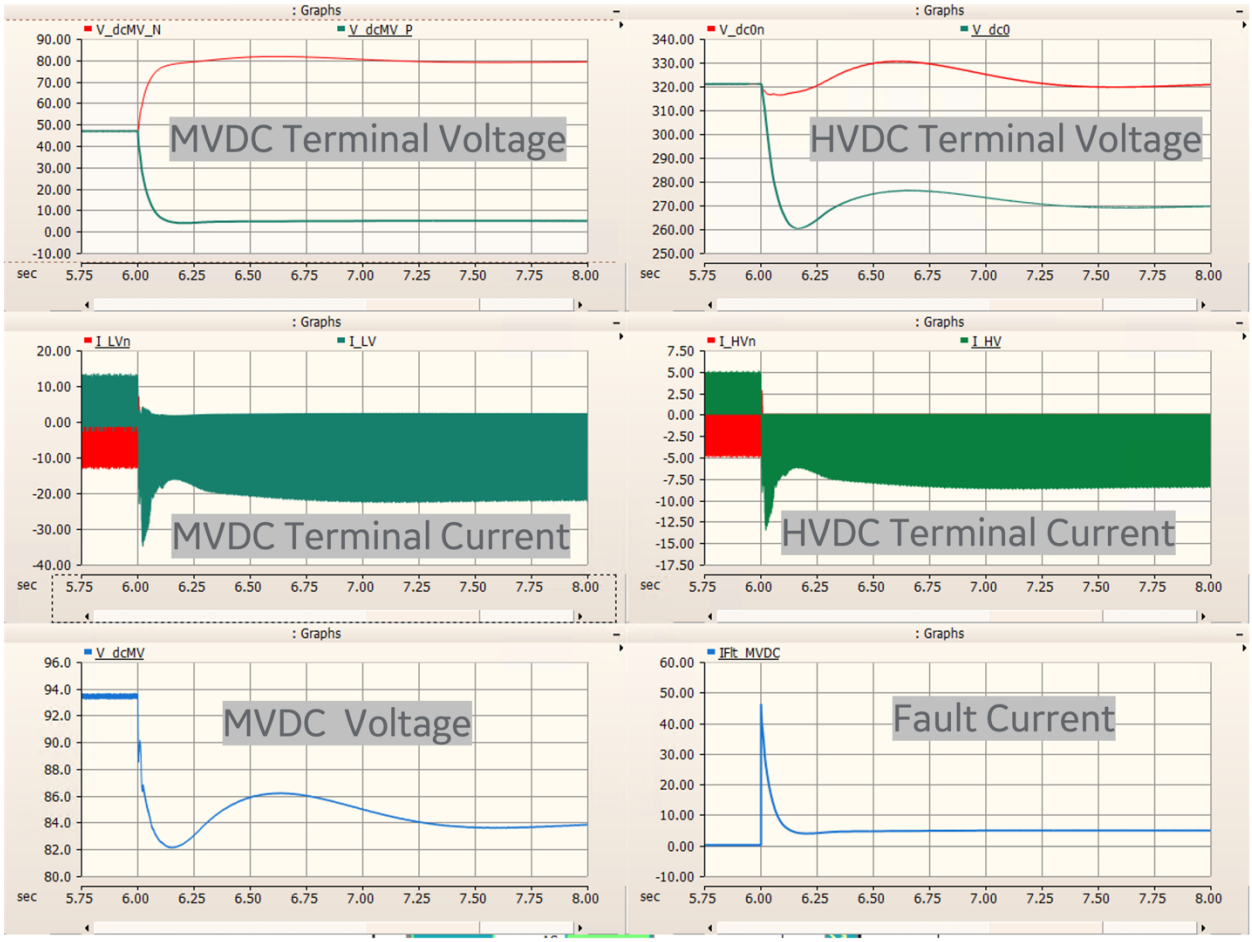

3.7 Potential Challenges and Key Takeaways

There are a few potential challenges for the MVDC-HVDC architecture:

1. MMC-based MVDC-HVDC power conversion can adopted from MMC-based HVDC converters, but the utilization of semiconductor rating is sub-optimal due the ac circulating currents which are required to balance arm energy.

2. Switched capacitor based MVDC-HVDC power conversion will need new development needed for high voltage & high-power applications; it will also require higher MVDC voltage to be efficient and a smaller number of devices due to its fixed voltage ratio; it will also need additional circuits for fault current blocking.

3. For MVDC output wind turbines, uncontrolled diode bridge can work together with existing MV step-up transformers at higher frequency to reduce the size or weight of the transformer. However, this will add another stage of power conversion and hence reduce the efficiency. Another solution is to use high-frequency dc-dc transformer which can directly step up the turbine dc bus voltage to MVDC level. However, such technology has relatively low technology readiness level (TRL).

4. There are also some other technical challenges such as MVDC cables and protections devices which need to be further studied.

4 Architecture Trade-offs

4.1 LCOE as the Cost-Benefit Analysis Criterion

Levelized Cost of Energy (LCOE) has been used to compare the cost of the different configurations of the wind farm as explained in the previous sections. LCOE reflects the minimal cost of generating electricity throughout the plant lifetime. It is an economic assessment criterion that allows to compare the cost of generating electricity from different assets of a same region therefore applying the same financial and economic assumptions including cost of goods, labor, and services, taxes, credits, etc. LCOE includes all the costs over the plant lifetime: initial investment, financial charges, cost of fuel, maintenance, fuel, tax credits, operation performance, etc. A detailed LCOE calculation is rather cumbersome and usually not necessary in a conceptual phase of a project as it requires many detailed cost inputs that are not always available or accurately known. Simplified LCOE calculations are often more practical especially when it comes to compare competing solutions as in the case of this cost-benefit analysis of the MVDC/HVDC proposed architecture. The following simplified LCOE formula has been applied for the analysis:

$$\mathbf{LCOE = \{(CapEx * WACC) + OpEx\}/AEP}$$

where CapEx is the total capital investment measured in dollars ($); WACC the weighted average cost of capital or financial charge for simplification in percentage per year; OpEx the average operation and maintenance expenditure measured in dollars per year ($/yr), and AEP is the average annual energy production measured in megawatt-hour (MWh). AEP is the product of the plant nominal capacity in MW, the average annual hours of operation, the system efficiency at the point of interconnection, and the plant net capacity factor. The total number of hours of operation can reflect the plant availability if that parameter is available otherwise a full calendar, 8760 hours can be used for simplicity. Typical offshore wind farms availability is >95% and this number is improving thanks to better technology design, maintenance planning, monitoring and diagnostics.

It is important to note the in our analysis renewable energy tax credits or other state or federal incentives have not been considered. The costs assumptions are based on projections for a plant entering service in 2035-2040.

AEP and Net Capacity Factor:

AEP is directly tied to net capacity factor of the wind farm. Capacity factor for wind turbine is a function of both the wind turbine rotor size (blades length) and the strength of the wind resource at the turbine location. Indeed, the wider surface area covered by the blades in motion the more wind energy can be

captured harvested. Similarly, the further the plant is from the shoreline the stronger the wind speed is typically. It is important to note that capacity factor can increase much faster with greater distances to shore as the energy potential of a wind turbine increases with wind speeds to the power of three. Capacity factor is therefore expected to be larger for the same turbine when it is installed deeper into the sea. Net capacity factor is the capacity factor at the plant level which is slightly lower due to the presence of multiple turbines and their impact on the wind flow distribution. Additionally, not all the turbines blow at the same speed at the same time especially in a large wind farm. For fixed bottom wind farm in North Atlantic Ocean (600 MW wind farm with 100 6 MW wind turbine), the net capacity factor is reported to be 48.8% in 2019 at a distance of 50 km (or 31 miles) from the shore [16]. Studies on offshore wind have reported capacity factors in the US of 46% by 2022 and 58% by 2028 [17]. As larger turbines such as the GE +12MW Haliade-X will become available and offshore wind plants will go deeper into the sea to harvest more energy thanks to technology development for new foundation and structure such as floating offshore, it is expected that capacity factor will continue to increase. In our analysis, a 12 MW wind turbine has been considered and net plant capacity factors of 47% and 54% have been estimated for distance to shoreline of <50 miles and >70 miles respectively.

WACC:

The after-tax weighted average cost of capital (WACC) is one of the most important components of the LCOE. It represents the average rate corresponding to finance charge of the capital investment for the plant. The WACC can represent a significant contribution. For our analysis as cost projections were based on a plant entering service in 2035-2040 the WACC was estimated at 6.25% according to [18].

CapEX:

CapEx is the total of capital investment to build the plant. It includes all costs associated with the construction of the offshore platforms, procurement, transportation, and installation of the wind turbines, the electrical and structural balance of plants, engineering, management, and commissioning of the project. Based on [16], the capex breakdown can be as per categories shown in Table 11.

1. **Turbine Cost**: In addition to the cost of the turbine structure (tower, nacelle, and blades assembly), all other cost associated with the wind turbine including its foundation, port logistics and transportation as well as installation are included in the Turbine cost. This is to simplify the cost table as the turbine and its associated costs do not change for all the architectures investigated.

2. **Electrical BOS material cost:** These costs are further classified into costs related to collection or inter-array cable, offshore substation, transmission or the export cable, and onshore substation. The breakdown of this cost category is shown in Table 11**Error! Reference source not found.**. It is important to note as explained previously that unlike HVAC transmission, HVDC transmission does not require reactive power compensation for voltage regulation and power factor compliance. Reactive power compensation costs are included accordingly to the requirement based on the export cable length. Costs estimates are referred from [2], [16], [19], [20], [21] including [22] for the estimate of the 320 kV DC offshore cable. Some components costs were only available for onshore. In those case they were adjusted to reflect an increase for offshore applications.

Table 11. Cost breakdown for CapEx

Turbine
Turbine (Tower and Rotor-Nacelle)
Turbine foundation
Turbine install
Port logistics and transportation
Electrical BOS (material)
Inter-array cable
Offshore substation
Transmission cable
Onshore substation
Structure BOS
Topside structure
Foundation
Onshore structure
Electrical assembly and installation
Cable installation
Port logistics and transportation
Substructure and foundation
Engineering & Proj management
Engineering & Development
Project management
Soft Cost

Table 12. Electrical infrastructure component for (a) MVAC collection – HVAC transmission system, (b) MVAC collection – HVDC transmission system, (c) MVDC collection – HVDC transmission system.

Components	MVAC collection – HVAC transmission	MVAC collection – HVDC transmission	MVDC collection – HVDC transmission
Inter-array cable	66 kV MVAC	66 kV MVAC	46/64/80 kV MVDC
Offshore substation	66 kV CB 220 kV CB GIS sw gear for 66 kV GIS sw gear for 220 kV 66/220 kV 450 MVA trf Reactor	66 kV CB 220 kV CB GIS sw gear for 66 kV GIS sw gear for 220 kV 66/220 kV 450 MVA trf 1.2 GW HVAC/HVDC MMC	DC Switchgear 1.2 GW MVDC/HVDC MMC
Export Cable	220 kV HVAC transmission	320 kV bipolar HVDC transmission	320 kV bipolar HVDC transmission
Onshore substation	220 kV CB 220 kV Disconnect AIS sw gear for 220 kV AIS sw gear for 500 kV Control room: relay SCADA 220/500 kV 400 MVA trf Reactive power compensation	1.2 GW HVDC/HVAC MMC 345 kV CB 345 kV Disconnect AIS sw gear for 345 kV AIS sw gear for 500 kV Control room: relay SCADA 345/500 kV 400 MVA trf	1.2 GW HVDC/HVAC MMC 345 kV CB 345 kV Disconnect AIS sw gear for 345 kV AIS sw gear for 500 kV Control room: relay SCADA 345/500 kV 400 MVA trf

3. **Structure BOS cost**: This includes the topside structure and the foundation of the offshore substation as well as the substructure of the onshore substation. The onshore substation cost is referred from [20] while the corresponding cost for the offshore is referred from [16] for conventional HVAC transmission. For the proposed MVDC/HVDC architecture costs were scaled for the offshore substation in proportion to the electrical infrastructure cost w.r.t. the conventional HVDC transmission. The cost of the onshore substation remains the same for both the proposed MVDC/HVDC technology and the conventional HVDC. Indeed, the two architectures can use the same VSC MMC technology for the grid interface inverter.

4. **Electrical assembly and installation cost**: This cost includes both the collection and export cables installation cost, port logistics and transportation cost as well as the substructure and foundation installation cost for the system except for the turbines. When only total installed costs were available material and installation costs were estimated to be in the ratio of 3:2 accordingly

from [2]. It is important to note that when it comes to the offshore infrastructure both material and installation unit costs ($/kW) are sensitive to the distance to shore. Material can increase due to distance (cables) or volume or weight (foundation) deeper into the ocean while installation and transportation are affected by longer vessels trips to access the plant and return to shore. Assembly & installation costs for most components are referred from [16].

5. **Engineering and project management cost**: This cost includes the engineering and development as well as the project management cost and is referred from [16]. For the proposed technology these costs are assumed to be similar to conventional HVDC as only the collection system and the offshore are affected, as the turbines, HVDC export cable and onshore substation remain the same. HVDC technology is per project basis and even conventional technology requires thorough engineering.

6. **Soft costs** include cost for insurance during construction, decommissioning bond, construction finance, sponsor contingency, and project commissioning. From [16], the soft cost is ~19% of the total BOS cost of both the fixed bottom as well as the floating wind farm example cases reported based on the data from the US offshore/onshore wind installations with HVAC architecture. Considering an increased hardware for the HVDC transmission architecture, soft cost is estimated to be 22% of the total BOS cost for DC interconnection.

OpEx and other variables:

OpEx is the operating cost, essentially for the renewable based systems it is the maintenance cost for the power plant. From [17] OpEx is expected to reduce from 93.1 $/kW/yr to 43.1 4/kW/yr from 2022 to 2028 for US offshore wind installations. For this study, an OpEX of 93.1 $/kW/yr is considered for the conventional HVAC architecture. Assuming the OpEx is dependent on the system infrastructure, OpEx for the DC interconnection is scaled based on their corresponding CapEx.

In LCOE formula, the annual energy yield (AEP) is dependent on the electrical efficiency of the system. Based on the load flow simulations performed, system efficiency for the AC interconnection scenarios is estimated at 95.8% and 95% when export cable lengths are 30 miles and 70 miles respectively. For the DC interconnection scenarios, the system efficiency is 96% and up to 96.9% for the conventional HVDC and the proposed technology. With the DC interconnection, transmission losses are considerably reduced as there being no charging current on the cable, therefore no reactive power losses associated. For the proposed technology, the efficiency is slightly higher thanks to loss saving with DC collection and the transformer-less MVDC/HVDC offshore converter. Details of the cost breakdown are given in Table 13.

4.2 Results of the LCOE Evaluation

Table 13 shows the cost of each category of the CapEx with inputs and references as discussed in previous subsection. Some further assumptions are added in the footnote to provide context of the estimate. All the costs are unit cost given in $/kW obtained from cost and size of the project in reference. The total CapEx used for the LCOE is the sum of all the categories as shown in the last row.

Table 13 Cost breakdown of the CapEx of a baseline offshore wind farm of 1,200MW for different scenarios of interconnection. (a) 66kV AC collection / 220kV AC transmission for 30 miles, (b) 66kV AC collection / 220kV AC transmission for 70 miles, (c) 66kV AC collection / ±320 kV DC transmission for 70 miles, (d) ±80kV DC collection / ±320kV DC transmission for 70 miles

Cost breakdown in $/kW	MVAC-HVAC – 30 miles	MVAC-HVAC – 70 miles	MVAC-HVDC – 70 miles	MVDC-HVDC – 70 miles
Turbine	1838	2028	1838	2028
Turbine (Tower and Rotor-Nacelle)	1100	1100	1100	1100
Turbine foundation	646	967	808	808
Turbine install	71	106	89	89
Port logistics and transportation	21	31	31	31
Electrical BOS (material)	305	518	407	323
Inter-array cable@	109	109	109	71^
Offshore substation	31	36	134	86^^
Transmission cable@	112	314	59	59
Onshore substation	53	59	106	106
Structure BOS	170	215	408	366
Topside structure	108	108	217	186
Foundation	42	83.5	83*	72*
Onshore structure	20	24	108*	108*
Electrical assembly and installation	279	507	286	263
Cable installation@	178	355	121	121
Port logistics and transportation	37	57	81*	70*
Substructure and foundation	64	96	83*	72*
Engineering & Proj management	208	218	229	252
Engineering & Development	138	145	156	176
Project management	70	73	73	76
Soft Cost	560	806	739	706
Total CapEx	**4033**	**5366**	**4917**	**4731**

@ Cable material cost is estimated 60%, and installation cost to be 40 % of the total cost associated with the cable and is added in 'Electrical BOS' and 'Electrical assembly and installation' sections respectively. Cost of HVAC for 70 miles is scaled by the distance as well as the ampacity is increased for longer distance due to higher charging current, so thicker copper conductors are required. The cost is accordingly estimated.

* Collected from different GE internal sources

^Collector system layout is assumed to be same as the MVAC collection (i.e., length of the collection cable is 166 miles). Peak of 66 kV AC is 54 kV, so a 66 kV AC cable is equivalent to 50 kV DC (bipolar), but current rating for each of 2 conductors for MVDC is higher than each of 3 conductors. However, the cost of 46 kV bipolar DC cable (2 conductors without ground) is scaled accordingly w.r.t the 66 kV AC 3-core cable (3 conductors).

^^Calculated for 3 different medium voltage with 3, 2 and 1-stage SiC based DC-DC converter. The cost is scaled based on the conventional MMC inverter cost.

Table 14 and Table 15 show the results of the LCOE analysis for different interconnection scenarios of a baseline case offshore wind farm of 1,200MW located in the US northeast coast. Cost inputs are based on medium term projections for plants entering commercial operation in 2035-2040. The analysis shows in Table 14 scenarios of a plant close to shore with export cable length ~30 miles and in Table 15 a plant distant from shore with an export cable length ~70 miles. The export cable length represents the distance between the offshore substation and the grid interconnection point onshore which may not be necessarily at the shoreline. Results confirm that for short interconnection distances (<50 miles), conventional AC transmission with HVAC export cables allow to obtain a lower LCOE than DC transmission. Indeed, for a plant capacity factor of 47% at ~30 miles to shore the LCOE obtained with HVAC transmission and HVDC transmission are $92.6/MWh and $101.7/MWh respectively. However, for longer transmission distances (>60 miles) results clearly confirm that DC interconnection is the only viable option as it allows to obtain a LCOE of $90.1/MWh with conventional HVDC compared to $99.4/MWh with AC transmission. With the proposed technology the LCOE can be further improved and reduced to $87.5/MWh with ±46kV DC collection and up to $85.9/MWh with a ±80kV. Higher DC collection voltage allow to optimize the inter-array cable cost and efficiency of the collection with no reactive power losses unlike in AC collection.

Results reveal that LCOE at greater distances to the shoreline can be lower than closer to the shoreline. It is important to note that this is only due to greater capacity factors anticipated at deeper distances into the ocean. Indeed, if with the same turbine and rotor size the plant capacity factor does not improve deeper into the sea there will be no reason to extend the export cable and therefore the plant should be installed the closest possible. The capacity factor correlation with distance to shore revealed to be a critical parameter for the plant installation and adoption of the interconnection technology. The section below further details the analysis.

Table 14. LCOE for a 1.2GW offshore wind farm at ~30 miles to shore with different scenarios of interconnection

Parameters	MVAC-HVAC, 66kV AC	MVAC-HVDC, 66kV AC
CapEX ($/kW)	4,033	4,434
OpEX ($/kW/yr)	111.7	122.59
Plant capacity factor	47%	47%
Efficiency	95.8%	95.9%
AEP (MWh/yr)	4,712,992	4,717,912
LCOE ($/MWh)	**92.6**	**101.7**

Table 15. LCOE for a 1.2GW offshore wind farm at ~70 miles to shore with different scenarios of interconnection

Parameters	MVAC-HVAC, 66kV AC	MVAC-HVDC, 66kV AC	MVDC-HVDC, 46 kV DC	MVDC-HVDC, 64 kV DC	MVDC-HVDC, 100 kV DC
CaPEX ($/kW)	5,367	4,917	4,798	4,760	4,731
OpEX ($/kW/yr)	148.7	136.2	132.9	131.8	131.1
Plant capacity factor	59%	59%	59%	59%	59%
Efficiency	95.0%	96.0%	96.5%	96.7%	96.9%
AEP (MWh/yr)	5,842,044	5,905,384	5,935,824	5,948,000	5,960,176
LCOE ($/MWh)	**99.4**	**90.1**	**87.5**	**86.6**	**85.9**

4.3 Discussions

It is well known that DC transmission is more cost-effective than AC transmission for long distance cables. Cables have a large capacitance which in AC generates significant reactive power proportional to their length. When increasing the length, the reactive power generated increases which decreases the maximum active power that can be transmitted through the same conductor cross-section. Therefore, to be still able to transmit the power generated by the plant either the conductor cross-section is increased or more export cables are installed in parallel. Both solutions significantly increase the transmission costs beyond the proportional increase of the distance. In addition, transmission losses also significantly increase. Moreover, because of the variation of the power generation, voltage along the transmission cables largely fluctuates which requires installation of reactive power compensation as demonstrated in section 1.5. Figure 39 shows the cost comparison performed between AC and DC interconnections for different export cable lengths confirming that beyond a certain distance (~50 miles), DC transmission becomes more economical than AC transmission despite the cost of the converter stations at both end of the transmission cables.

The plant distance to shore affects the LCOE of offshore wind farms in many ways. On the one hand it impacts the costs of foundation structure as it relates to the water depth, installation, and transportation of goods which are significant components of the capex. On the other hand, it can impact the capacity factor which directly affects the total energy generation. In the northeast coast for instance, the capacity factor will notably increase for the same turbine and rotor size (blades length) the deeper the plant is into the sea. This is due to greater wind speeds available deeper into the ocean which allows to harvest more energy as compared to plants closer to the shore.

Figure 39 Cost comparison between Conventional HVAC and Conventional HVDC architectures with varying distance from the shore

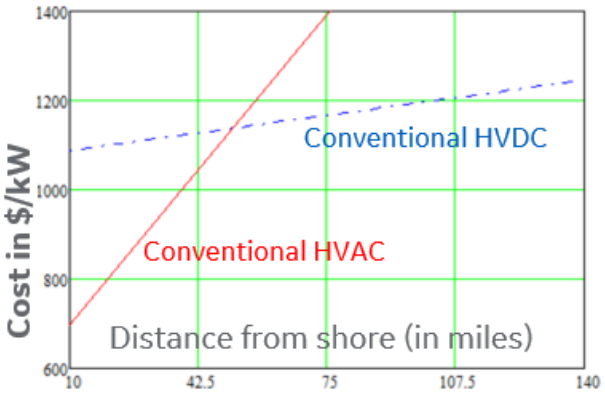

Our analysis indicates that if installing the same plant at 70 miles as opposed to 30 miles can increase the capacitor factor by 25% (from 47% to 59%), the LCOE of the plant becomes comparable to short distance from shore while generating 25% more electricity. This is a very strong argument for deep water offshore wind farms installation and the use of HVDC transmission. This suggests that fewer plants need to be installed to meet the renewable energy targets. In other words, cost of electricity can be reduced by adopting deeper water installation as enables by HVDC transmission. Our proposed MVDC/HVDC interconnection technology allows to reduce the LCOE even further. Indeed, with various DC collection voltage the LCOE ranges between $87.5/MWh and $85.9/MWh, a reduction of up to 4.7% as compared to conventional HVDC transmission. The proposed technology allows to reduce LCOE by essentially reducing the electrical balance of plant cost and losses at the collection system. Indeed, by adopting a DC collection system, the cost of inter-array cables and their installation can be reduced by up to 34%. However, the key differentiation of the proposed topology resides in the offshore converter which allows to generate the HVDC voltage for transmission without the use of power transformers. This saves weight and footprint on the offshore platform which overall allows reduce the costs of the structure and foundation as shown in Table 13. The different DC collection voltages evaluated suggest that ±80kV DC

output at the turbine allows the lowest LCOE which over 20 years lifetime can generate an energy cost saving of ~$496 million compared to conventional HVDC transmission.

A sensitivity analysis has been performed using the ±80kV DC collection configuration to evaluate how the cost of the key components specific to the proposed technology affects its LCOE performance as compared to conventional HVDC. Table 16 shows the ratio between LCOE of the proposed technology and that of conventional HVDC for different cost scenarios including a +/-25% variation of the cost of the offshore converter substation for both; +/-50% variation in the MVDC or the MVAC collection. Those three components were selected as they are specific to the two compared technologies. Indeed, even though other components such as the turbine, the platform structure, the onshore substation, or HVDC export cables have relatively a strong contribution to the LCOE their costs are not different for the two technologies therefore will not reveal much on their relative LCOE performance.

Table 16. Comparison of the LCOE of the proposed technology and conventional HVDC under different parameters

		MVDC Converter cost		
		down 25%	*baseline*	*Up 25%*
HVDC MMC cost	25% down	0.95	0.97	0.99
	baseline	0.93	0.95	0.96
	25% up	0.92	0.93	0.94
MVDC cable cost	50% down	0.92	0.94	0.95
	baseline	0.93	0.95	0.96
	50% up	0.94	0.96	0.97
MVAC cable cost	50% down	0.94	0.96	0.98
	baseline	0.93	0.95	0.96
	50% up	0.92	0.93	0.95

The analysis shows that in all the scenarios considered, the proposed technology offers a lower LCOE than conventional HVDC. Indeed, under a wide variation of the estimated cost inputs, the ratio between the LCOE of the proposed MVDC/HVDC technology and conventional HVDC remain <1, suggesting that the LCOE can be further reduced with the proposed technology if the DC collection system or the MVDC/HVDC converter can be optimized. Notably, if the cost of the MVDC/HVDC converter can be reduced by 25%, the proposed technology will reduce LCOE by up 7% as compared to conventional HVDC. This corresponds to an LCOE of $83.8/MWh and an energy cost saving of $745 million over 20 years lifetime of the wind plant.

In summary, the proposed MVDC/HVDC offshore architecture is a viable solution to reduce LCOE of offshore wind as it allows to reduce the interconnection costs of distant wind farms (>50 miles). Plants at greater distances to the shore typically get access to higher wind resources which can significantly increase their capacity factors with the same nominal power rating. This therefore helps accelerate penetration of offshore wind by reducing its LCOE and increasing its energy contribution with interconnection of high-capacity factors wind farms. Overall, the required capacity of offshore wind to meet the energy targets for decarbonized power grid can be reduced. The novel proposed converter has the advantage to not require transformer which increases the power density and reliability of offshore platforms while reducing the maintenance costs. Additional development is necessary to further optimize the design and validate some critical technical performances including the converter control, fault interruption strategy, and system reliability.

5 References

[1] "2018 Offshore Wind Technologies Market Report," [Online]. Available: https://www.energy.gov/sites/prod/files/2019/09/f66/2018%20Offshore%20Wind%20Technologies%20Market%20Report.pdf.

[2] "Prysmian Group," 1 October 2021. [Online]. Available: https://na.prysmiangroup.com/press-release/vineyard-offshore-wind-farm-project-moves-forward-as-first-large-scale-offshore-wind-farm-in-the-us. [Accessed 26 April 2022].

[3] A. McBride, "Vineyard Wind Offshore Wind Generation and Transmission Project (QP 700) - Proposed Plan Appliations," ISO-NE, 4 January 2021. [Online]. Available: https://www.iso-ne.com/static-assets/documents/2021/01/vineyard_wind_offshore_wind_generation_and_transmission_project_qp700_vineyard_wind_i_3_9_letter_vw_20_g01_vw_20_t01through_vw_20_t05.pdf. [Accessed 26 April 2022].

[4] ABB, "XLPE Land Cable Systems User's Guide Rev 5," ABB High Voltage Cable Unit, 2010.

[5] ABB, "XLPE Submarine Cable Systems Attachment to XLPE Land Cable Systems - User's Guide Rev 5," ABB High Voltage Cable Unit, 2010.

[6] P. Kundur, Power System Stability and Control, McGraw Hill, 1994.

[7] E. Muljadi, S. Pasupulati, A. Ellis and D. Kosterov, "Method of equivalencing for a large wind power plant with multiple turbine representation," in *2008 IEEE Power and Energy Society General Meeting*, 2008.

[8] FERC, "Reactive Power Requirements for Non-Synchronous Generation," 23 June 2016. [Online]. Available: https://www.federalregister.gov/documents/2016/06/23/2016-14764/reactive-power-requirements-for-non-synchronous-generation. [Accessed 26 April 2022].

[9] ISO-NE, "OP 19 Appendix K - Operating Voltage Limits by LCC," 1 April 2022. [Online]. Available: https://www.iso-ne.com/static-assets/documents/rules_proceds/operating/isone/op19/op19k_rto_final.pdf. [Accessed 26 April 2022].

[10] ISO-NE, "ISO New England Operating Procedure No. 12 - Voltage and Reactive Control," 24 March 2022. [Online]. Available: https://www.iso-ne.com/static-assets/documents/rules_proceds/operating/isone/op12/op12_rto_final.pdf. [Accessed 26 April 2022].

[11] ABB, "HVDC Light Cables - rev. 2006-04-10," ABB High Voltage Cable Unit, 2006.

[12] "Sunrise Wind Will be First Offshore Wind Project in United States to Use HVDC Transmission Technology," [Online]. Available: https://sunrisewindny.com/news/2021/10/sunrise-wind-will-be-first-offshore-wind-project-in-united-states--to-use- hvdc-transmission-technology. [Accessed May 2022].

[13] J. D. Páez, J. Maneiro, S. Bacha, D. Frey and P. Dworakowski, "Influence of the operating frequency on DC-DC converters for HVDC grids," in *2019 21st European Conference on Power Electronics and Applications (EPE '19 ECCE Europe)*, 2019.

[14] G. J. Kish, M. Ranjram and P. W. Lehn, "A Modular Multilevel DC/DC Converter With Fault Blocking Capability for HVDC Interconnects," *IEEE Transactions on Power Electronics,* vol. 30, pp. 148-162, Jan, 2015.

[15] H. TAGHIZADEH, C. BARKER and R. WHITEHOUSE, "Current Control Circuit". Patent WO/2020/164901, Jan 2020.

[16] T. Duffy and P. Stehly, "2019 Cost of Wind Energy Review," National Renewable Energy Labs, Dec, 2021.

[17] Y. Shimeng, L. Søren and K. Rolf, "Global bottom-fixed Offshore Wind LCOE," Wood Mackenzie, October 2019.

[18] EIA, "EIA LCOE Outlook 2022," [Online]. Available: https://www.eia.gov/outlooks/aeo/pdf/electricity_generation.pdf. [Accessed 23 12 2022].

[19] T. Duffy and P. Stehly, "2020 Cost of Wind Energy Review," National Renewable Energy Laboratoty, Jan, 2022.

[20] "Transmission Cost Estimation Guide for MTEP22," Midcontinent Independent System Operator (MISO), April, 2022.

[21] "Mongolia: Energy Efficiency and Urban Environment Improvement Project," HJI Group Corporation, United States in association with Richwell Engineering LLC, Mongolia, December 2018.

[22] Prysmian, "320kV DC offshore cable," [Online]. Available: https://www.prysmiangroup.com/en/media/press-releases/prysmian-awarded-more-than-%E2%82%AC-800-m-for-two-offshore-wind-farm-grid-connection-cable-systems-in-germany. [Accessed 23 12 2022].